LASER & PHOTONICS REVIEWS

Laser Photonics Rev. **5**, No. 3, 422–441 (2011) / **DOI** 10.1002/lpor.201000023

Abstract Semiconductor lasers are the most efficient man-made narrow-band light sources and convert up to three-quarters of electric energy into light. High-power diode lasers are characterized by very high internal power densities in their small cavity, resulting in local heating and sometimes device degradation. Catastrophic optical damage (COD) of diode lasers is a relevant degradation mechanism and limit for reaching ultra-high optical powers. An overview is given on research activities targeting the mechanisms being relevant for the COD process in GaAs-based diode lasers emitting in the 630–1100 nm range. The discussion of experiments, where COD is artificially provoked, represents the main topic. The sequence of events and fast kinetics taking place on a nanosecond to microsecond time scale are addressed. A particular emphasis is laid on recent experimental work performed in the authors' laboratories. Paving the way for knowledge-based solutions towards more robust diode lasers represents the ultimate goal of this work.

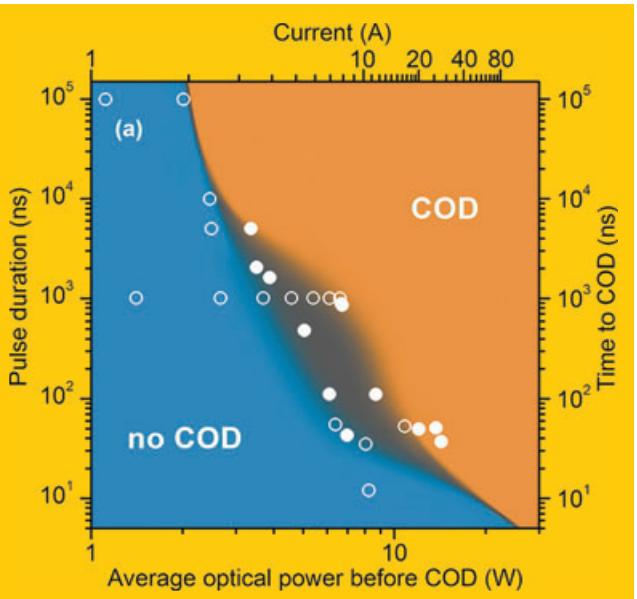

COD diagram determined for a batch of broad-area AlGaAs diode lasers. The time to COD within a single current pulse is plotted versus the actual average optical power in the moment when the COD takes place. Full circles stand for clearly identified COD events (right ordinate), whereas open circles (left ordinate) represent the pulse duration in experiments, where no COD has been detected. A borderline (gray) exists between two regions, i. e., parameter sets, of presence (orange) and absence of COD (blue). This borderline is somewhat blurred because of the randomness in filamentation of the laser nearfield and scatter in properties of the involved individual devices.

Mechanisms and fast kinetics of the catastrophic optical damage (COD) in GaAs-based diode lasers

Jens W. Tomm[1,*], Mathias Ziegler[1,2], Martin Hempel[1], and Thomas Elsaesser[1]

1. Introduction

1.1. COD and thermal runaway

Semiconductor lasers, the most efficient man-made narrow-band light sources, convert up to 73 percent of electric energy into light [1] and reach kilowatt output powers from one single monolithic array [2]. High-power operation is inherently connected with very high internal power densities of up to 10^{10} W/cm^3 within the quantum well (QW) representing the core component of the optical active region. The power not converted into light causes a strong local heating and might eventually even lead to device failure.

Among a variety of degradation processes, catastrophic optical damage (COD) is a particular sudden failure mechanism occurring in edge-emitting diode lasers. It is observed at elevated emission power levels and involves a substantial or total loss of optical output power. COD is connected with an optically induced structural change, i. e., damage of the device, sometimes even a physical destruction of the surface at one of the facet mirrors of the laser cavity. The latter failure mode is sometimes called catastrophic optical mirror damage (COMD) and can be observed by optical inspection or scanning electron microscopy (SEM). The emission power (or power density) at which COD starts is frequently called *COD threshold* (P_{COD}). COD must not be confused with other sudden failure mechanisms due to current leakage paths or due to lack of gain which occur without optically induced damage. The efforts of telecommunication industry to manufacture highly reliable high power pump lasers has led to decisive breakthroughs in understanding the failure mechanisms of short wave semiconductor lasers [3].

Figure 1a shows the structure of an edge-emitting high-power broad-area (BA) diode laser. For achieving best cooling, it is soldered with the epitaxial layer that contains the optically active QW region to a heat sink. Figure 1b shows a commercial 808 nm emitting device with its front (outcoupling) facet directed to the reader. Optical micrographs of the front facet of a pristine device and after COD are given in Fig. 1c and d, respectively. Maps of laser emission (the

[1] Max-Born-Institut für Nichtlineare Optik und Kurzzeitspektroskopie, Max-Born-Str. 2A, 12489 Berlin, Germany
[2] Current address: BAM Federal Institute for Materials Research and Testing, 12200 Berlin, Germany
[*] Corresponding author: e-mail: tomm@mbi-berlin.de

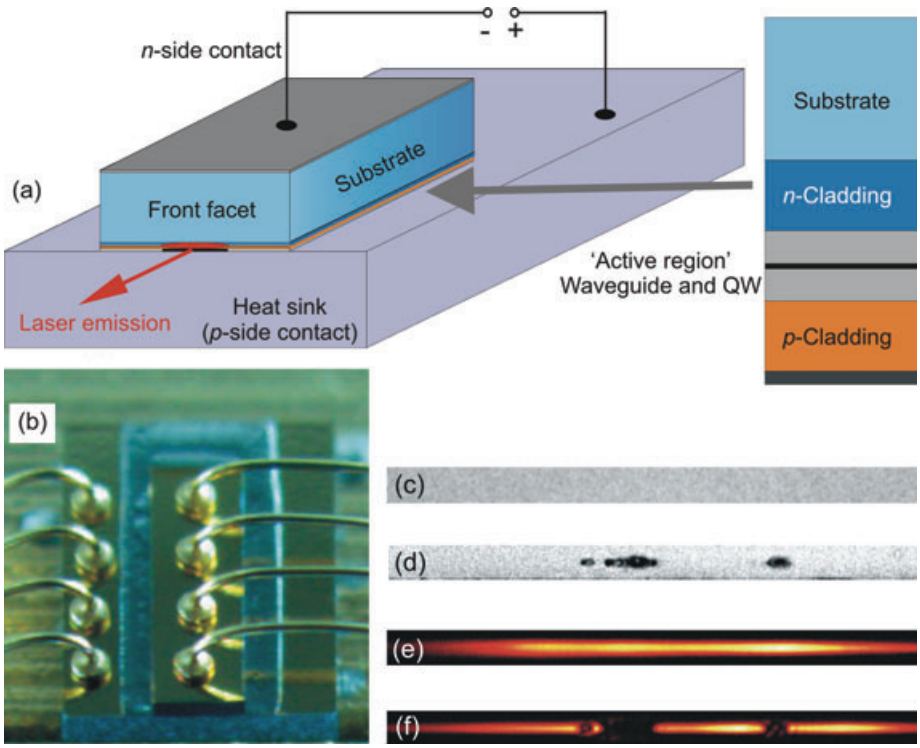

Figure 1 (online color at: www.lpr-journal.org) (a) Schematic of a high-power diode laser (left) and of the epitaxial layer system (right). (b) Micrograph of an 808 nm emitting high-power diode laser. The device is packaged onto a submount (bluish). Four wires in center provide the n-current supply. The front facet with the dimensions 400 µm in width and 100 µm in height appears black. Micrographs of the about 1 µm thick optical active region representing a small part of the front facet before (c) and after COD (d). Spatial distribution of the laser emission (nearfield) at an operation current of 0.5 A from the same device before (e) and after COD (f).

so-called *optical nearfield*) from the same device before and after COD are given in Fig. 1e and f.

COD is known since the first implementation of diode lasers [4–6]. As early as 1973 Eliseev characterized it as a microexplosion [7]. In 1979, Henry et al. [6] published a comprehensive work addressing COD, its root causes, and the expected kinetics. Most of the ideas presented in these early studies are still valid and describe COD to be jump-started by a fast *thermal runaway* [6], which is initialized by an elevated facet temperature, and eventually results in a microexplosion [8–10]. The thermal runaway phenomenon with the critical temperature has been for first time measured by Tang et al. [11] with an external heating source. This paper was a milestone in the understanding of the thermal runaway, as it showed for the first time a direct measurement of the critical temperature. Later, it was shown that extrinsic effects such as surface recombination and the creation of structural defects are involved in the absorption and temperature rises as well, and eventually even dominate [8, 12–15].

Figure 2 describes the thermal runaway as it can happen either at the facet or anywhere in the bulk of the device. The starting point is an elevated temperature at the facet or at any other location within the laser cavity. The relevant heating mechanisms at the facets are, e. g., surface recombination [16] and surface currents [17]. Within the cavity, re-absorption of laser light at defects can cause elevated local temperatures. In addition, the type of packaging may result in enhanced facet temperatures: diode lasers are often packaged with an 'overhang' (of the semiconductor chip with respect to the heatsink) of some 10 µm in order to protect the front facet from solder material. Thus, a facet temperature elevated relative to that of the average bulk can

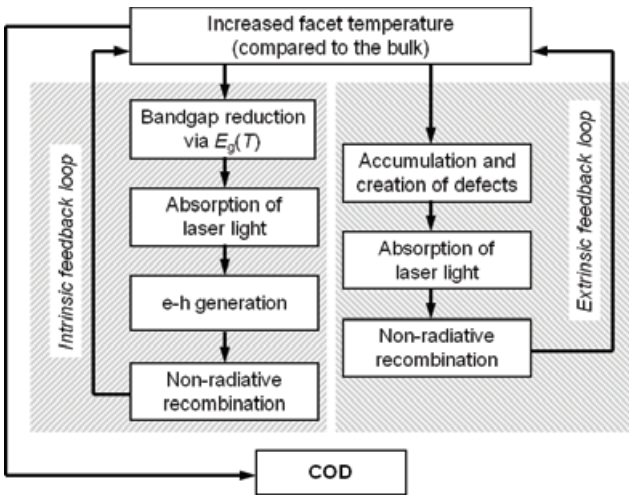

Figure 2 Schematic diagram of the sequence of events during COD.

occur below and above the lasing threshold, even in absence of any high-power operation or presence of defects [18]. When increasing the temperature further by increasing the operation current and/or the heat-sink temperature, or by long term operation resulting in aging-induced defect creation, a critical local temperature T_{crit} may be reached. At this point, both intrinsic and/or extrinsic mechanisms which lead to an additional temperature increase, create positive feedback loops and the *thermal runaway* sets in.

The *intrinsic* loop leading to device failure (left-hand side of Fig. 2), has been described by Henry [6]. Elevated temperatures cause a bandgap shift $E_g(T)$ of the semiconductor materials near the surface. Thus, the interband ab-

sorption (at the laser emission wavelength) increases in this region, resulting in a higher density of non-equilibrium carriers close to the surface. This will cause additional heating, even for a constant fraction of non-radiatively recombining carriers, and a positive feedback loop is set into action by this mechanism. For QW-based active regions, the modal absorption is about two orders of magnitude smaller than for bulk material which represents the active region in early heterolasers. Thus, the re-absorption of laser light in a heated facet region is expected to be reduced by the same amount. Hope was drawn from this fact to eliminate COD in QW lasers [19]. However, the effect remained relevant. As pointed out by Chen and Tien [12], the barrier or waveguide material of QW lasers can be involved in the intrinsic feedback loop. Potentially, free carrier absorption can also contribute to the formation of an intrinsic feedback loop.

The *extrinsic* feedback loop is shown on the right-hand side of Fig. 2. Elevated temperatures are known to promote defect accumulation and creation. Defect accumulation at the facets or at any other heated location within the laser cavity results in an increased absorption of laser light via defect-related optical transitions (e. g., bound-to-free) or in absorption due to extended or even macroscopic defects. The term *non-radiative recombination* is used for describing the subsequent energy transfer from the defect site to the semiconductor lattice. This energy transfer represents an additional source of heating, closing an extrinsic feedback loop. Reports on lowered COD thresholds in aged diode lasers [20–23] indicate the existence of this type of feedback loop. The re-ignition of the thermal runaway by subsequent current pulses [24, 25] represents an indirect evidence for this behavior. COD schemes similar to Fig. 2 have been published by several other authors as well [9, 12, 14, 21, 26, 27].

Although the two main feedback loops are addressed here separately, combinations of the two scenarios occur: the *intrinsic* thermal bandgap shrinking increases the *extrinsic* absorption via shallow defects the absorption cross sections of which are energetically coupled to $E_g(T)$. In practical devices, various types of feedback loops are likely to coexist for different operation conditions. In all cases, heating activates a temperature-enhanced process that causes additional heating, resulting in positive feedback. The subsequent microexplosion is spatially confined for energetic reasons: the emission power, the only source feeding the thermal runaway process, decreases after the onset of COD and impairs the device.

In this review, special emphasis is laid on the sequence of events leading to an irreversible damage of laser devices and on the underlying physical mechanisms. The following terminology is used: the term *COD* describes the entire degradation process, which leaves the device partially or completely damaged. The term *thermal runaway* is used for the period when the positive feedback loop causes the fast heating process (Fig. 2). Before the thermal runaway starts, a *critical temperature* T_{crit} must be reached. There are three phases of COD:

I. The facet temperature approaches T_{crit}. Experimentally determined values are $T_{crit} = 120$–140 °C [11,17,19,28], 150 °C [29] and 160 °C [30]. This phase ends when the thermal runaway starts in a small area of a facet or in the bulk.
II. The thermal runaway takes place as illustrated by the scheme given in Fig. 2. This phase involves the *melting process* and also the *spatial extension* of the hot spot. This phase ends, when the runaway stops because of a lack of energy [15].
III. Further degradation occurs if the pump current is not instantaneously switched off, representing the standard situation in practice. Thus, this phase might involve also the creation of *collateral damage*.

This review mainly addresses the *fast processes* around the thermal runaway. It should be noted that it is still unclear whether a single COD scenario exists for all types of devices. This lack of systematic knowledge is mainly due to the tremendous variety of diode lasers, material systems, device designs, and operation conditions. Conclusions presented in the literature are based on results obtained with specific devices and combining lines of arguments given by different authors involves the risk to put incomparable things together. Therefore this overview is limited to GaAs-based devices emitting in the 6XX-11XX nm range. COD in short-wavelength GaN- and long-wavelength InP- based devices as well as in quantum-cascade lasers is not addressed here. The reviews/books by Eliseev [9, 31] and Fukuda [27] both cover a substantially wider scope of the earlier literature.

The main reason for dealing with COD is the quest for strategies to avoid this effect. Although a proper choice of operation conditions reduces the chance to provoke COD, the key strategy is an improvement of device fabrication technology. In the following Sect. 1.2, a brief overview of the technical options to reduce the probability of COD occurrence is given. The related technologies are mostly protected by patents with many details being confidential. Thus, this part will remain incomplete, all the more as it will be referred preferably to peer-reviewed literature. Overviews focusing on important technological aspects including the rich patent literature are given, e. g., by Harder [3].

1.2. Robustness of diode lasers against COD

After diode lasers have been created at the beginning of the 1960ies, the facets were soon identified as a major bottleneck for their reliability. A substantial improvement has been achieved by the deposition of facet coatings in the 1970ies. Such coatings, which are, e. g., made of Al_2O_3, allow for controlling the reflectivities of front and rear facets and lead to a substantial increase of P_{COD}.

The era of high-power diode lasers began at the end of the 1980ies [32, 33]. In particular, the research on diode laser facets for single-mode lasers at IBM is well documented [11, 17, 19, 20, 29, 34–40]. After having identified the root cause of COD in lasers with as-cleaved (uncoated) facets as a temperature-activated surface-chemical reaction, several surface passivation technologies [36, 41–43] have been successfully developed in order to shift P_{COD}-values towards higher emission powers. The so-called $E2$ technology [36] involves in-vacuum cleaving of the laser facets

with subsequent passivation by the low-energy deposition of Si [43]. Comparable approaches involve deposition of Ge, Al, or Sb [43, 44]. Alternatively, the cleaving of the facets may take place in air or in an atmosphere of an inert gas. Both approaches, however, require additional cleaning, e. g., by ion-beam [45] or hydrogen-plasma etching [16], and passivation, e. g., by nitridation [46] or sulphation [41, 47, 48]. Extra processes such as InGaP- or ZnSe-epitaxy [42, 49] are applied as well. Additional methods for increasing the COD threshold are:

- *Non-injecting mirrors* [14, 50–53]. This approach relies on the reduction of the current density (and thus carrier concentration) at the front facet. Current blocking stripes located at the front facet of the laser represent one option, while packaging with overhang is even simpler.
- *Non-absorbing mirrors* [54–62]. This approach, sometimes called *window laser*, involves the artificial reduction of the modal absorption of the close-to-facet gain material. In a QW, this can be accomplished by implantation and thermal treatment. This process, called *QW intermixing* [63], shifts the laser transition towards higher photon energies and produces the desired reduction of the modal absorption.
  Another option to achieve lower modal absorption near the facets is the use of tensile strained QWs. The component of the originally biaxial built-in strain of the QW which is perpendicular to the facet plane is expected to vanish at the facets. Relaxed tensile strain leads to a blue shift of the QW absorption, i. e., a reduced modal absorption at the lasing wavelength.
- Higher COD thresholds can be achieved by a reduction of the facet load in terms of power density. The so-called *large optical cavity* concept [64, 65] involves a widened waveguide and, thus, a vertically extended area of interaction between laser light and facet. 'Super large optical waveguides' are discussed [66], and even thicker waveguides are involved in 'photonic crystal laser structures' [67].
- *Low optical confinement* or *large spot size* structures [60, 68] rely on a regular waveguide which is widened in the vicinity of the facet. In this way the actual power densities at the facet are reduced. This holds also for 'slab-coupled optical waveguide laser' structures [69–71] where higher-order modes are selected from an otherwise multimode rib waveguide to an adjacent slab region.
- Different *material systems* show different sensitivities to COD [9, 72]. If possible, even the proper choice of the material system can help reaching higher P_{COD} values.

An early overview on P_{COD}-values for various devices, material systems, and operation conditions has been given by Eliseev [9]. The state-of-the-art is represented by continuous wave (cw) COD thresholds of P_{COD} per aperture width of 285 mW/µm [65]. This corresponds to a power density of about 30 MW/cm^2.

The following chapters will not deal with these important technical solutions for improving COD hardness. Instead, the main topics are the mechanisms and sequence of events during the COD process. This requires analytical experimental work based on *destructive* and *non-destructive* methods. Figure 3 illustrates the outline for the following chapters. In chapter 2, experiments where COD is intentionally provoked are discussed. Devices are destroyed and information is derived from the operation conditions leading to COD and from the resulting damage pattern. Chapter 3 addresses (potentially) non-destructive methods, which are applied mainly to the first phase of COD, before the thermal runaway starts physical destruction. Chapter 4 returns to fully destructive experiments which involve an *in situ* analysis of the sequence of events during the process and allow for resolving COD in time.

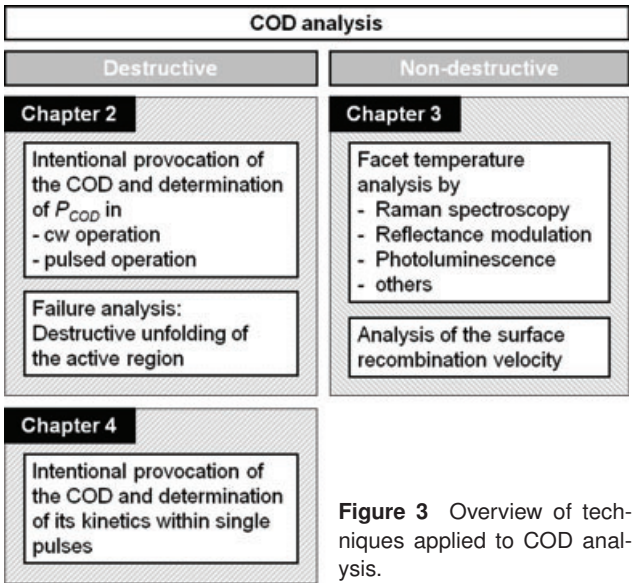

Figure 3 Overview of techniques applied to COD analysis.

2. COD testing and destructive analysis

2.1. COD threshold in cw operation

COD appears either as one among other sudden degradation mechanisms during long-term cw aging [27, 31], or it is intentionally provoked. The latter is typically achieved by measurements of the output power versus operation current ($L-I$) towards high current values. Typically, an $L-I$ measurement takes a few minutes and the devices reach a *steady-state thermal condition* for each current value. In this respect, a slow current sweep is equivalent to a cw experiment. Figure 4a shows the results of such measurements for a homogeneous set of red-emitting devices as reported by BouSanayeh [73]. The abrupt power fall-offs which are marked by arrows, clearly point to the COD thresholds P_{COD}. Beyond COD, the lasing power does not drop to zero but remains at a value specific for a device batch. While P_{COD} drops with increasing heat-sink temperature, the current at which COD takes place increases. This is due to the strong temperature dependence of the slope efficiencies of these particular devices. At a heat-sink temperature of 40 °C, one observes the so-called *thermal rollover* instead of COD. This behavior illustrates that the critical facet temperature $T_{facet} = T_{crit}$ is not reached under such conditions. There are

two contributions to T_{facet} [73, 74], i. e.,

$$T_{facet} = T_{bulk} + \Delta T\,. \tag{1}$$

Here, T_{bulk} represents the average temperature within the laser cavity, which is typically estimated from the diode lasers emission wavelength, and ΔT represents the additional temperature increase of the active region close to the facet, which is almost proportional to the emission power. For a heat sink temperature of 40 °C, T_{bulk} is increased, but the emission power is reduced, resulting in a smaller ΔT. The absolute value of this reduction is obviously larger than the increase of T_{bulk}. Eventually, the maximum T_{facet} (40 °C) remains below T_{crit} and COD is absent. The same test done for pulsed operation is expected to provide a different result because of the changed ratio between T_{bulk} and ΔT.

This example shows how P_{COD} can be determined experimentally. It also demonstrates that the result depends very much on the operation conditions. Furthermore, P_{COD} depends on packaging that defines (among others) T_{bulk}. The experimental results in Fig. 4a illustrate the need to separate contributions to T_{bulk} from those related to ΔT, e. g., by additional test in pulsed operation. Experimentally, T_{crit} is estimated from facet temperature measurements just before COD [13, 75] as will be discussed in Sect. 3. Typical values reported are T_{crit} = 120–140 °C [11, 17, 19, 28], 150 °C [29] and 160 °C [30].

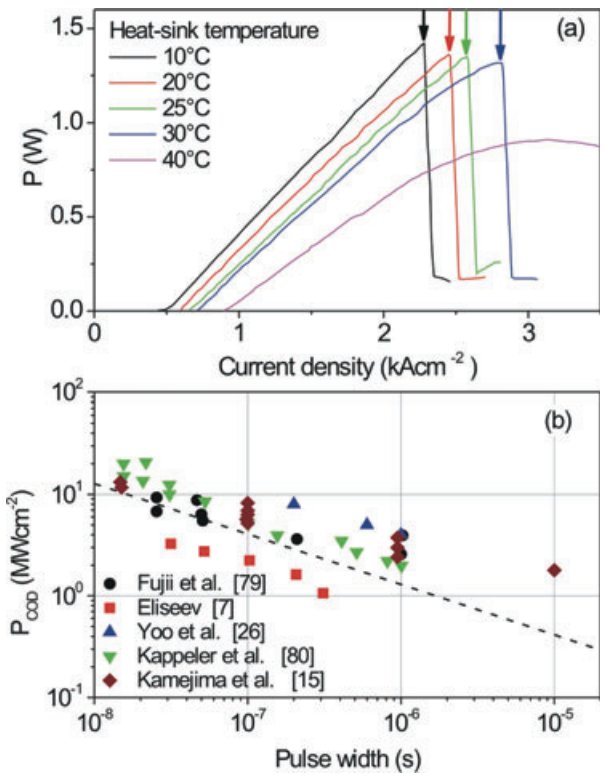

Figure 4 (online color at: www.lpr-journal.org) (a) L-I curves of five BA AlGaInP lasers for heat-sink temperatures between 10 and 40 °C. COD is marked by arrows. (b) P_{COD} versus pulse length data taken from different references. The slope of the dashed line represents the 'square-root law'.

COD may appear as a sudden degradation mechanism in genuine cw experiments, i. e., during long-term aging [29, 38, 76]. This is phenomenologically explained by step-by-step lowered P_{COD} levels due to gradual degradation of the semiconductor material close to the outcoupling facet. If the actual emission power is kept constant ('constant power aging'), P_{COD} will gradually decline to the emission power and at this point the thermal runaway sets in. In a more microscopic picture, the road towards COD in long-term cw experiments is explained as follows: gradual degradation creates defects within the semiconductor material adjacent to the facet. Absorption of laser light at these defects progressively increases the value of T_{facet}. Thus, even for a constant power level T_{facet} rises continuously [20, 77] and the thermal runaway starts at $T_{facet} = T_{crit}$. A quantitative description of the route towards T_{crit} during cw operation has been provided by Moser et al., employing an Arrhenius analysis [29, 38, 78]. Such an approach is very common in reliability analysis for describing gradual and thermally activated aging processes [27]. It relies on the assumption that the gradual process which pushes T_{facet} towards T_{crit} is the only (or major) gradual degradation mechanism being relevant for the investigated type of devices. The *time to COD* (t_{COD}) is determined for different power densities P_d. The relation

$$\frac{1}{t_{COD}} = \nu \cdot \exp\left(-\frac{E_a}{c \cdot P_d}\right) \tag{2}$$

has been applied to derive a linear progression of data points. The parameter 'thermal energy' cP_d pinpoints P_d as driving force for achieving an enhanced facet temperature. E_a is an activation energy and ν an Arrhenius parameter. This description allows for statistical lifetime estimates of device batches. The authors performed this type of analysis also for sets of devices that experienced various facet treatments, and drew conclusions on the surface chemistry of facet degradation [29].

2.2. COD threshold in pulsed operation

The situation during pulsed operation is more complex. Here, the temperature contributions relevant for reaching $T_{facet} = T_{crit}$, namely T_{bulk} and ΔT, can be by varied in a wider range than in the cw case by selecting appropriate parameters of the current pulses. In most reports the repetition rate is kept low in order to minimize the T_{bulk}-value at the beginning of each pulse. COD tests have been performed for various pulse lengths by successive increase of the pulsed operation current in $L-I$-type measurements. Figure 4b summarizes the results obtained by several authors by plotting P_{COD} versus the pulse length [7, 15, 26, 79, 80]. Although the data stem from different devices and from different reports, the general behavior of the batches is similar. The tendency is well described by the 'square-root law' $P_{COD} \sim \tau^{-0.5}$ (τ : pulse length) discovered by Eliseev [7] and confirmed and thermally modeled by Kappeler et al. [80] (dashed line). For long pulses (right bottom

part in Fig. 4b), one approaches the cw situation. For short pulses (left top part in Fig. 4b), P_{COD} increases substantially. As semiconductor lasers do not store energy (in contrast to other types of lasers), the increase of P_{COD} for short pulses is considered a pure thermal effect.

Lock et al. [81] investigated the COD behavior of 980 nm emitting devices by applying hydrostatic pressure during pulsed operation. This enabled them to study the intrinsic wavelength dependence of COD. It was shown that the wavelength dependence of P_{COD} can be explained in terms of the reduction in mode size with increasing pressure (decreasing wavelength) as a result of the increase in the optical confinement factor.

There are reports addressing the possibility of multiple thermal runaways during pulsed operation [15, 82–85]. Up to now, this possibility has been discussed *ex post* only on the basis of results obtained by transmission electron microscopy (TEM) of devices that were mechanically opened after COD. The obtained micrographs display a discontinuous propagation of defect zones along the cavity axis including the formation of periodic defect loops. In concert with the pulsed operation mode, this periodicity has been considered to pinpoint the possibility of multiple thermal runaway ignitions. Kamejima et al. [15] reported experiments, where the devices have been subjected to a defined number of pulses. The TEM micrographs obtained from the resulting defects show the same number of defect loops. This suggests that they are caused by multiple thermal runaway ignitions. This finding is interesting, because re-ignitions of the runaway are expected to be based on processes belonging to the extrinsic feedback-loop of the process (Fig. 2). Only recently Hempel et al. [24, 25] have given direct evidence for multiple ignitions by monitoring the presence of the runaway process during subsequent pulses by thermography.

2.3. Failure analysis of devices affected by COD

Any sudden failure can easily be detected if the emission power is properly monitored in an $L-I$-type measurement as shown in Fig. 4a. After a sudden failure, it must be figured out whether the observed degradation is COD-related indeed. Optical inspection of the facets is helpful for making assignments and sometimes clear degradation signatures are visible (Fig. 1d). In other cases, even careful SEM inspection does not reveal any surface alteration [77], whereas electroluminescence patterns reveal darkened areas not far behind the seemingly unaffected facet. If COD signatures are visible at the facet, there is typically a correlation between P_{COD} and the observed surface damage, i. e., the higher P_{COD} the more extended the damage pattern at the facet [86, 87].

In addition to the facets, COD may affect the bulk of the device, in particular the QW gain medium inside the laser cavity. Such damage can be mapped in photo- (PL) or cathodoluminescence (CL) patterns of the QW plane. For this purpose, the devices are opened mechanically by removing the *p*- or *n*-contact metallizations and – in *p*-down packaged geometries – the substrate. PL or CL maps are taken

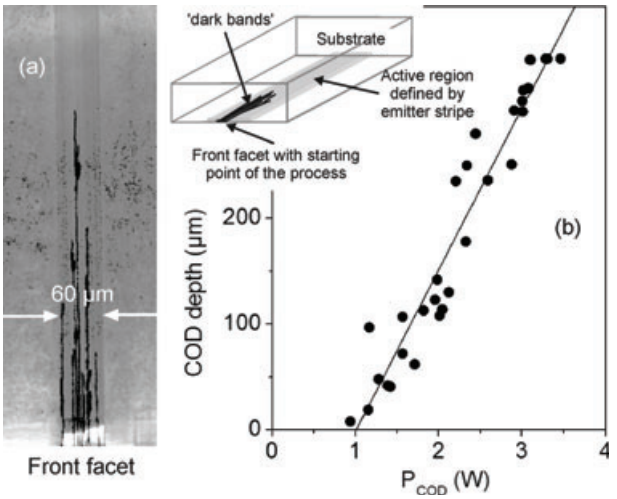

Figure 5 (a) CL map of the QW emission from an emitter stripe of a BA laser, which failed by front facet COD during cw operation according to [77]. The inset depicts the geometry of the propagation of the *dark band*s along the cavity. (b) Length of the dark bands versus COD threshold as measured by Pendse [96] when driving cw 30 individual BA diode lasers into COD.

either as panchromatic maps or at the QW emission wavelength. COD generates areas of substantially reduced QW emission in such maps, the so-called *dark bands* [85, 87–97]. The barriers, into which the QW is physically embedded, are typically less or even not affected by this type of damage. The occurrence of *dark bands* is considered an experimental proof for COD as an active failure mechanism. Figure 5a shows a typical CL map of the QW emission from an emitter stripe of a BA laser which failed by front facet COD during cw operation [77]. The inset depicts the geometry of the damage within the cavity. Figure 5b shows a plot of the length of the *dark bands* versus COD threshold as measured by Pendse [96], when driving 30 individual BA diode lasers during cw operation into COD. This clear correlation shows that the penetration depth of the dark bands into the cavity depends on the energy available when COD ignites and that both *external* and *internal* damage correlate with P_{COD}.

Even without direct experimental proof, there is not much doubt in the literature that the melting temperature (T_m) is at least momentarily reached during the thermal runaway. On the other hand, it is not clear if the formation of *dark bands* along the QW also requires reaching T_m. Snyder et al. [85] pointed out that this propagation might take place even at lower temperatures assuming that it is driven by a small metal-rich (Ga, In) region which is created during the thermal runaway. This zone of material with comparably low T_m travels through the crystal which has a substantially higher T_m-value.

The spreading direction of the *dark bands* is defined by the propagation direction of the optical mode rather than by the crystallographic orientation of the semiconductor crystal [93, 98]. This finding shows that the reabsorbed laser light acts as the main driving force. This is further confirmed by reports that refer to *ring-cavity modes* being involved in the formation of dark bands in BA lasers [93]. Nevertheless,

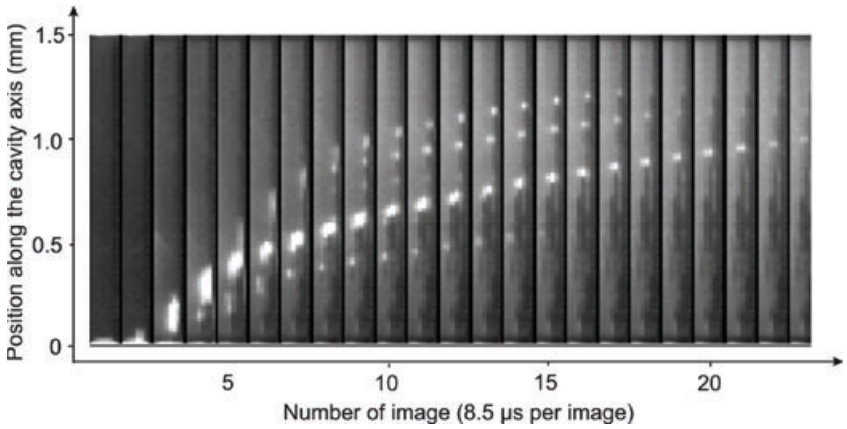

Figure 6 23 sequential images following the initiation of a COD according to Jacob et al. [92]. The optical cavity is imaged through a top window in the *n*-contact of the substrate of the 808 nm emitting BA-laser. The COD initiates at the front facet (position '0') and propagates toward the back. Each image is 8.5 µs in duration. The device failed to emit stimulated emission after ∼ 160 µs.

additional heating is expected from spontaneous emission and potentially from a local electrical short-cut created by local melting in the thermal runaway phase. Notice the conductivity of GaAs to increase by a factor of 26 upon melting [99]. Local electrical heating occurs in such highly conducting areas and could be effective also later, when the dark bands are created. In this period, the aforementioned metal-rich droplet could serve as an electrical bridge across the *pn*-junction.

The formation of dark bands has been directly monitored [92, 100, 101]. Using emission microscopy, Jacob et al. [92] took images of the active region plane in 808 nm cw operating BA lasers through the GaAs substrates with windows in the top contact. Figure 6 shows 23 images of the laser stripes monitored one after the other after the onset of COD. The integration time for each image was 8.5 µs and the first 0.2 ms after the onset of the thermal runaway are covered. *Bright spots* are visible, propagate, and separate into at least 5 branches. According to the authors, the spots are due to 'scattering of the laser light from the molten semiconductor region of the COD'. Laser light at 808 nm does, however, not penetrate through a 100 µm thick GaAs substrate. Therefore, the observed bright spots are likely to rather represent a type of defect emission [102]. Its link to the propagating COD front, however, is beyond any doubt, and it is highly likely that their motion along the laser axis marks the generation of the aforementioned *dark bands*. Park et al. [100, 101] have traced motions of *bright spots* in 980 nm emitting devices through a top window even over minutes. This was done in low-duty-cycle pulsed operation at loads not much higher than for cw operation.

Jacob et al. [92] determined a propagation velocity of 20 µm/µs immediately after COD ignition (cw) which slowed gradually down to zero at 160 µs, when device operation terminated. Other reports derive somewhat lower propagation velocities from damage patterns. Hakki et al. report 2–4 µm/µs [103], Kamejima et al. give 3–5 µm/µs [15], Ueda (and references therein) quote 1–5 µm/µs [84], Elliott et al. [86] find 5–13 µm/µs, and Mallard et al. determine 10 µm/µs and estimate 25 µm/µs as an upper limit [104]. The much smaller defect propagation velocities of µm/h observed in QW diode laser structures [105], represent genuine dislocation propagation velocities without substantial influence of high optical loads.

The crystallographic structure of the *dark bands* is described as polycrystalline [90, 93]. This suggests that they originate from a re-crystallization process. The starting point of the *dark bands* is not necessarily a facet. A structural defect inside the cavity may also serve as the origin. We consider such an internal sudden degradation phenomenon also COD as long as the initialization of the defect propagation involves the thermal runaway fed by the laser emission energy.

3. Non-destructive COD analysis

3.1. Facet temperature analysis

Although sounding paradoxical at first sight, non-destructive analysis of COD is feasible and useful. Most experimental methods rely on temperature measurements, in particular *facet temperature measurements during diode laser operation*. This approach is mainly motivated by the fact that T_{crit} plays a key role for the onset of the thermal runaway. Another type of COD-related analysis focuses on the surface status, e. g., by determining the surface recombination velocity at the laser facet (without laser operation). This survey starts with T_{facet}-measurements.

The following methods have been employed for an analysis of T_{facet}:

- Lattice temperature measurements by Raman spectroscopy, i. e., by detecting the temperature-induced changes of Raman spectra of lattice excitations (*phonons)*.
- PL or techniques of reflectance spectroscopy, e. g. reflectance modulation or thermoreflectance, to determine the impact of temperature to the *electronic* bandstructure.
- Thermography to detect *Planck's radiation* and derive temperatures. Such methods are straightforward but complicated, in particular in semiconductors being transparent in the infrared region.

The thickness of the active region of a diode laser consisting of the waveguide and the embedded QW (and barriers) amounts to *one µm* or less. The area of the device probed in the facet plane should not exceed this dimension in lateral direction. The 'information depth' of the applied technique should allow for detecting the true surface temperature. Consequently, the shape of the thermal profile

along the laser axis defines the requirements to be fulfilled by the method. Menzel [106] calculated a more than 20 percent ΔT-reduction after 1 µm along the laser axis, while Eliseev [9] and Chen et al. [12] found values even in the sub-µm range. Epperlein et al. determined a 1/e T-decay-length from the front facet temperature along the laser axis of 6 µm by analysis of electroluminescence spectra [39]. This corresponds to a ΔTreduction of 20 percent within the first 1.4 µm. Facet temperature measurements in concert with energy-balance considerations [107] revealed that the thickness of the heated region cannot exceed the order of one µm. Thus, any method for T_{facet}-analysis should have a lateral resolution and an 'information depth' of *one µm or better*.

The methods for measuring T_{facet} are presented in Sects. 3.2 to 3.4, followed by a brief discussion of studies of surface recombination.

3.2. Raman spectroscopy

The use of Raman spectroscopy as a 'surface thermometer' for diode lasers has been pioneered by Todoroki et al. [108]. Raman spectroscopy is an established analytical tool based on the analysis of scattered (external laser) light [109]. Among others, phonons represent the elementary excitations relevant for the inelastic scattering process. Since cleaving of (100)-oriented standard GaAs substrate material results in (110) facet planes, *transverse optical phonons* are of special relevance according to the Raman selection rules. Typically, several sets of such phonons are detectable which belong to the different binary sublattices of the active region materials such as the GaAs- and AlAs-sublattices for waveguide made of $Al_xGa_{1-x}As$. The relaxation of selection rules due to size effects in multilayer structures and to particular experimental issues such as the use of microscope objectives that cause non-perpendicular incidence can lead to the appearance of 'forbidden' phonon lines, e. g., of longitudinal phonons.

Phonon line positions and/or line intensities are extracted for an analysis of facet temperatures. Both parameters are affected by the lattice temperature via different mechanisms. Phonon line shifts are caused by the temperature dependence of the lattice constant (thermal lattice expansion modifies the phononic bandstructure). The intensities of Stokes- and anti-Stokes lines follow Bose-Einstein statistics. Line intensity ratios and spectral line shifts that may be extracted from the same spectra, allow for an independent extraction of facet temperatures and an agreement of both data sets represents a successful crosscheck [110]. In general, the temperature values determined from line shifts show a smaller scattering but might be systematically affected by strain causing an additional line shift. This can be an issue if packaging-induced strain relaxes with increasing temperature [111].

The required lateral spatial resolution is achieved by using a microscope. This approach is frequently referred to as *micro-Raman spectroscopy*. The 'information depth' along the laser axis is determined by the absorption coefficient of the active region material at the excitation laser wavelength. For the standard wavelength of 488 nm, the 'information depth' is about 100 nm. Thus, the criterion for a 'true surface temperature measurement' as addressed in Sect. 3.1. is fulfilled. Typical measuring times are on the order of 1–3 minutes for monitoring a complete micro-Raman spectrum. High-performance backside-illuminated CCD cameras for detection allow for data acquisition times of tenths of seconds.

In their early paper [108], Todoroki et al. reported facet temperatures of more than 200 °C, a value that clearly exceeds any possible bulk temperature of an operating diode laser. Moreover, they presented first temperature profiles across facets, and explicitly pointed to the potential of micro-Raman spectroscopy for COD analysis. Brugger et al. [34] detected ΔT-values of more than 400 K for degraded uncoated lasers (and mentioned values up to $\Delta T \sim 1000$ K). They compared temperatures of cleaved and coated facets and demonstrated an enhancement of the optical strength of coated facets by a factor of 4–5, due to the facet treatment applied.

Tang et al. [11] monitored COD directly and reported maximum values of $T_{\mathrm{facet}} \sim 700$ °C. They addressed the residual effect of excessive pump powers and reported temperature increases of up to ~ 600 K caused by this mechanism [112]. The same group investigated the dependence of T_{facet} on the cw operation current and the emission power at rather low currents around the laser threshold [17]. T_{facet} was found to scale with the current rather than with the emission power. Thus, their data implies that the facet heating during the first phase of COD is dominated by surface recombination. In another report, Tang et al. [19] compared the evolution of facet temperatures for QW- and heterolasers. Again they stressed the link between T_{facet} and the cw pump power for QW-lasers to be weak, in striking contrast to early heterolasers. This is in agreement with the by two orders of magnitude smaller modal absorption (and consequently re-absorption of laser light). Nevertheless, the COD process in present QW devices is still clearly driven by emission power.

Statistical analysis of T_{facet}-measurements for different BA device batches under cw high-power operation (1.7 W) has been reported by Tomm et al. [110]. This work allowed for a systematic comparison of different waveguide designs with respect to T_{facet} and - in this way - to their tendency to develop COD. T_{facet}-values of 100 °C have been found for large optical cavity step index structures while elevated values >130 °C are determined for graded index structures. Figure 7a shows theT_{facet}-evolution of a device being cw operated *en route* to COD [110]. Here, the measuring time of 200 s per data point impeded resolving any fast kinetics. The resulting temporal temperature-averaging is likely to be the reason that a temperature of only ~ 300 °C is found during the thermal runaway. A rather high temperature was observed as long as the device shows lasing. The temperature recovered to the T_{bulk}-value only after the device terminated any operation. Rinner et al. [52] used micro-Raman spectroscopy in order to proof the T_{facet}-reduction caused by the introduction of a current blocking layer at the front facets of their devices. Even the T_{facet}-increase due to long-term grad-

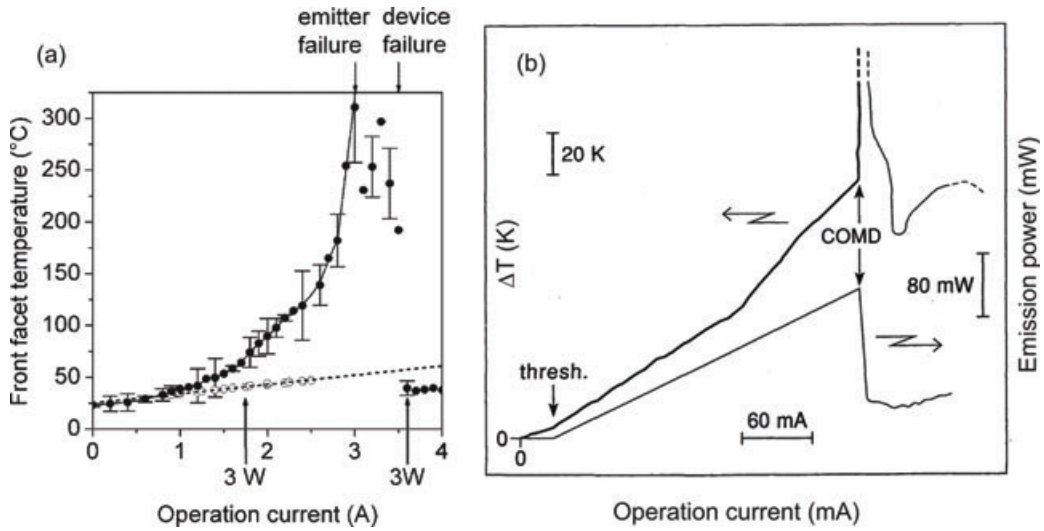

Figure 7 (a) Facet temperatures (full circles) of a central emitter of a high-power diode laser array versus cw operation current for a BA device according to Tomm et al. [110]. Open circles denote bulk temperatures obtained from laser emission data. The lines are guides to the eyes. Arrows at the top mark the failure events, whereas the arrows at the bottom give the operation current, where the thermal load of the device equals 3 W (left arrow before and right arrow after the failure event). (b) Mirror temperature (left ordinate) versus operation current of a 10 µm wide coated AlGaAs diode laser demonstrating the onset of COD at a critical temperature, according to Epperlein [118]. The operation power (right ordinate) versus operation current is given for comparison.

ual degradation (i. e., before COD) has been monitored [77]. A comparison of facet temperatures of QW and quantum-dot lasers of similar design indicated a lower T_{facet}-value for the quantum-dot devices [113].

Tomm et al. [114] quote typical errors of 20 K and 100 K for micro-Raman spectroscopy at ambient temperature and 500 °C, respectively. An accuracy improvement from 25 K to 5 K has been claimed by Abstreiter et al. [115, 116] by using the photocurrent generated by the excitation laser within the diode laser structure as help for the optical alignment of the Raman microscope.

3.3. Reflectance modulation and thermoreflectance

The *reflectance modulation technique* for measurements of facet temperatures has been pioneered at IBM Rüschlikon by Epperlein et al. [28, 35, 39, 117, 118]. This approach exploits the impact of T on the electronic bandstructure of the laser materials. The temperature-induced modification of the bandstructure results in temperature-induced changes of the reflectance spectrum, which are probed in the experiment. A key concept consists in finding a *probe wavelength* at which the reflectance is a strictly monotonic (typically increasing) function of temperature. This results in a well-defined relation between the *intensity* of the reflected light and the temperature. The 'right' probe wavelength is typically found in the blue range where the reflectance increases towards the E_1-transitions of the relevant materials [119]. Excitation wavelengths suitable for an analysis of $Al_{0.3}Ga_{0.7}As$-waveguides are 472 [71], 458 [117], or 442 nm [119]. Such short probe wavelengths also keep the 'information depth' well below 100 nm. The required lateral resolution is achieved with a microscope and lock-in detection schemes result in high detection sensitivities. The required *reflectance modulation* is typically achieved by temperature modulation of the investigated device via the operation current [28, 39, 57, 58, 117, 118, 120–122]. In contrast to the micro-Raman-approach, one records only two scalar quantities, namely R and ΔR at the particular wavelength (typically via two channels of the look-in amplifier)

$$T_{\text{facet}} \sim \frac{\Delta R}{R}, \tag{3}$$

reducing the measuring times substantially. The proportionality factor in Eqn. (3) depends sensitively on the probe wavelength and the inspected material and needs to be determined experimentally for each sample. Epperlein quotes a temperature uncertainty of the technique of 0.5 K [117], while Wawer et al. give a value of <1 K [123]. Additional temperature calibration of the reflectance modulation technique has been achieved by using micro-Raman data for the same devices [35, 119].

The unsurpassed speed of the measurement has allowed for the first studies of COD kinetics within reasonable measuring times. Figure 7b shows the T_{facet}-evolution of a device being cw operated *en route* to COD [118]. The onset of the fast degradation is unambiguously proven by simultaneous monitoring of the emission power (right ordinate scale). After the onset of the thermal runaway, a ΔT-increase of 330 K within less than 2 s is found. The high speed of the reflectance modulation technique allowed to take temperature maps at facets [28, 71, 117, 119, 120, 123–128]. Furthermore, it became possible to monitor even fairly extended devices such as high power diode laser bars, often called 'cm-bars' (because of the total array width of one cm) [126–128].

Bugajski et al. [125] have used this technique for analyzing different mounting arrangements via an advanced determination of thermal resistances and for the assessment of different etching technologies. The same group also reported facet temperature analysis in quantum cascade devices [123, 129]. Hayakawa et al. [120–122] investigated the impact of device design parameters such as emitter stripe width and waveguide thickness on the facet temperature. Piva et al. [57, 58] quantified the effect of QW intermixing to facet temperatures and found a substantially reduced facet temperature for devices with non-absorbing mirrors. Schaub et al. [130–132] have employed thermoreflectance spectroscopy for the separation of different factors affecting device efficiency and sensitivity to COD.

A substantial improvement in terms of data acquisition velocity has been reported by Chan et al. [71]. By using an *imaging approach*, the entire reflectance map of the front facet is monitored by a CCD-camera. Data from each pixel is averaged over many on-off cycles providing temperature and index maps. The same approach has been used for analysis of (bulk) thermal relaxation times of a quantum-dot diode laser, which are otherwise hardly accessible [124].

3.4. Further approaches for facet temperature analysis

There are a number of useful alternatives complementing the standard methods of micro-Raman and thermoreflectance spectroscopy. The application of PL for facet temperature analysis has been pioneered by Garbuzov [133–135]. It probes the electronic bandstructure, similar to reflectance measurements. While tracing the edge emission, red-shifts of the PL spectrum in a thermally loaded device are interpreted as thermally induced $E_g(T)$ shifts. Using the known or the separately measured $E_g(T)$-dependence, facet temperatures are determined. In contrast to micro-Raman and reflectance spectroscopy, the *results are influenced by carrier transport*, namely both by drift and diffusion. This involves interferences caused by band bending as well as lateral and in-plane diffusion. Even if a microscope objective is used for focusing and short-wavelength excitation keeps the penetration depth small, diffusion increases the 'information depth' to more than 1 µm. In addition, the heated facet region forms potential minima into which carriers are expected to drift. In practice, these effects can hardly be evaluated or separated in a quantitative way, resulting in a substantial systematic error of the absolute temperature values. On the other hand, the method is simple and often absolute facet temperatures are not required, but only a distinction between batches prepared in a different way. In order to circumvent any interferences with the diode lasers primary emission, front-facet-PL is probed from the barriers, the waveguide, the cladding layers, [21, 133–137] or even from the substrate [138]. PL spectra from these parts are sufficiently spectrally separated from the device emission, which is additionally suppressed by filters. Using micro-PL, Yoo et al. [136] showed the superiority of Al-free active regions compared to Al-containing ones with respect to the facet temperature. Chavan et al. [21] used PL measurements in order to prove facet degradation to be more severe for untreated as compared to passivated facets.

Other approaches to derive temperatures include measurements of spontaneous emission from the waveguide of a QW diode laser [133] and electroluminescence for temperature analysis along the cavity axis [139]. Moreover, Sweeney et al. [75] analyzed the high energy tails of the device emission. Assuming them to be caused by spontaneous emission from QW and waveguide, effective carrier temperatures were derived. Close to COD, T_{facet}-values of ~ 1000 °C have been estimated. Bertolotti et al. [140, 141] developed a *photo-thermal deflection* method for T_{facet}-measurements in different kinds of laser structures. Such data provide additional information on thermal diffusivity.

Thermography, the analysis of Planck's (black-body) radiation, is not suitable for probing surface temperatures. Neither the lateral spatial resolution nor the 'information depth' meets the requirements defined in Sect. 3.1., mainly because of the low absorbance (emittance) of the (thin) heated surface region and huge background contributions [142, 143]. Thermography has, however, been applied successfully for T_{bulk}-analysis [144–150]. Moreover, the thermal runaway in COD creates a 'thermal flash' of Planck's radiation which can be detected by thermography. Although this 'thermal flash' of infrared emission does not allow for any direct T_{facet}-measurement, it unambiguously indicates the onset of the thermal runaway and can be used for COD analysis [24, 74, 87, 151, 152]. This approach will be discussed in chapter 4.

3.5. Surface recombination and surface currents

If surface recombination represents a driving force for the initial facet heating indeed (Sect. 1.1), there should be a link to the COD behavior as well. Following Henry et al. [6] and Kappeler et al. [80], Yoo et al. [26] have modeled P_{COD} in dependence on the surface recombination velocity. The results have been compared with COD tests carried out with devices that experienced different facet treatments. The authors conclude that a reduction of the surface recombination velocity from 4×10^5 to 2.3×10^5 cm/s by an improved facet passivation process would increase P_{COD} from 4.8 to 10.3 MWcm^{-2}. A reduction of the surface recombination velocity to below 10^5 cm/s should prevent any thermal runaway.

The measurement of *surface recombination velocities* at diode laser facets is a complex experimental challenge. Standard methods such as transient free carrier gratings [153] or photocurrent spectroscopy [154] fail to give reliable numbers because of the small size and multilayer nature of the active region within the front facet plane, and/or because of the large number of additional unknown parameters being required for data analysis. Ziegler et al. [16] used transient micro-PL measurements with two different excitation wavelengths (i. e., 'information depths') in combination with model calculations for an analysis of surface recombination velocities at the substrate area of device facets. Values of $\sim 10^5$ and $\sim 10^6$ cm/s were determined for 'good' and 'poor'

facets, respectively. Micro-Raman measurements taken at the active region of the same devices confirmed the findings: below the laser threshold, the average ΔT was (4±1.5) and (11±4) K. At the threefold threshold current, ΔT_{facet} was (17±3) and (40±5) K, for 'good' and 'poor' facets, respectively. Although the substrate and the active region part of the facets are expected to underlie comparable surface chemistries, even this approach gives no direct access to surface properties of the active region.

There has been some speculation about the impact of *surface currents* on the COD behavior of diode lasers. In principle, surface currents could create a thermal runaway scenario as described in Sect. 1.1: surface heating reduces E_g close to the facet, leading to a reduced forward resistance of the *pn*-junction and an increased current density in this region. In this way, more heat is generated and a positive feedback loop is closed without any involvement of emission power. There are, however, arguments against this scenario: the formation of dark bands, and, in particular, the self-termination of this process in a partly damaged device are not compatible with a dominating role of surface currents. Clear experimental evidence of effects related to surface currents has only been given by Tang et al. [17].

4. COD kinetics

4.1. Theory and modeling of the kinetics

In Sect. 1.1, 3 phases of COD are defined, a first one during which T_{crit} is achieved, a second thermal runaway phase in which COD ignites, and a third final phase in which defect creation is still going on as long as the device is not turned off. The kinetics of the first phase are addressed, namely t_{COD}, the time for the attainment of T_{crit} in case of cw operation (Eqn. 2). This type of kinetics are rather 'slow', namely $t_{COD} = 10^{-3}$–10^{3} h, depending on the protection status of the facet and the emission power density. Thus, this type of 'COD kinetics' is considered a special type of gradual degradation. In this section it will be shown that t_{COD} can be 'compressed' by more than 10 orders of magnitudes to some 10 ns.

To our knowledge, experiments have not resolved the thermal runaway phase of COD (cf. scheme in Fig. 2) in time so far. There are theoretical predictions which will be addressed next. Eliseev [7] discussed the kinetics of the thermal runaway process and called it a 'self-damage' process. By using (analytical) one-dimensional modeling and assuming a temperature-dependent absorption coefficient at the lasing wavelength, he clearly pinpointed the thermal runaway process as the most likely to initiate the COD process. Henry et al. [6] modeled the width of the absorbing layer at a cleaved surface with a surface recombination velocity of $4{\times}10^5$ cm/s, irradiated by 5–15 MWcm^{-2}. In dependence on the flux, he found values of 10 ns $< t_{COD} <$ 100 ns for the time necessary to accumulate sufficient energy in this heated region for reaching T_m. The authors have shown, that the runaway takes place independent of the presence of defects as starting points of the process. For the runaway itself, representing the *fastest process within the COD sequence of events*, they found a substantial rise in temperature to occur within about 1 ns.

In a series of papers, Nakwaski [8, 155, 156] dealt with the theoretical description of COD based on the work of Henry et al. [6]. He combined for the first time 3-dimensional (analytical) modeling with the key assumption of a temperature dependent absorption coefficient and applied this to a realistic laser structure, namely a heterolaser with a cavity length of 400 µm and a stripe width of 8 µm. For this particular structure t_{COD} values of 6 and 500 ns were determined for operation currents of 4.5 and 0.8 A [8]. After this first step towards a realistic shape of the heat source within the facet plane, he waived the assumption of a flat heat source [155]. While the calculated t_{COD}-values are again on the order of some 10 ns, the more realistic shape of the heat source lead to a prolongation of the time, within which T_m is reached, to 'several nanoseconds'. Further refinements of the model such as the introduction of temperature dependent thermal conductivity and diffusivity have been reported in [156]. It was shown that a determination of an exact value of the critical mirror temperature T_{crit} is of minor importance from the catastrophic degradation point of view because the temperature increase is of an avalanche type. For the heterostructure described above, t_{COD}-values down to 2 ns have been predicted for currents of 50 A. More recent numerical simulations were reported by Smith [10]. For the particular parameters used t_{COD}-values of 10 ns are determined, while the thermal runaway is predicted to be very fast, namely $\Delta T > 300$ K in less than 1 ns.

Recently Miftakhutdinov et al. [157, 158] published complementary modeling work, where the impact of parameters such as surface recombination velocity, volume non-radiative recombination, facet coating, and waveguide absorption on P_{COD} is discussed. For the COD kinetics of their laser structures they found t_{COD}-values of 20 ns and 20 µs for power levels of 5 and 1.1 times the cw P_{COD}-values. The temperature rise during the thermal runaway has a value of 40 K/ns.

Since the thermal properties of the materials in diode laser architectures are well-known, all calculations provide comparable results. The main parameter controlling COD kinetics is the energy which is deposited into the small volume close to the front facet. For reasonable parameter sets, t_{COD} amounts to 1–100 ns, while the *thermal runaway* is expected to take place within <1 ns. One may conclude that Nakwaski's [156] statement on the minor importance of T_{crit} for the overall results of COD modeling can be extended also to the particular mechanisms involved into the thermal runaway.

4.2. Monitoring the kinetics of the COD process

The experimental methods discussed so far bear potential for temporally resolving COD kinetics. Now the time-resolved COD studies will be discussed in a systematic way. A 'real-time' COD study by scanning tunneling microscopy has been published by Cobley et al. [159]. It has been shown that

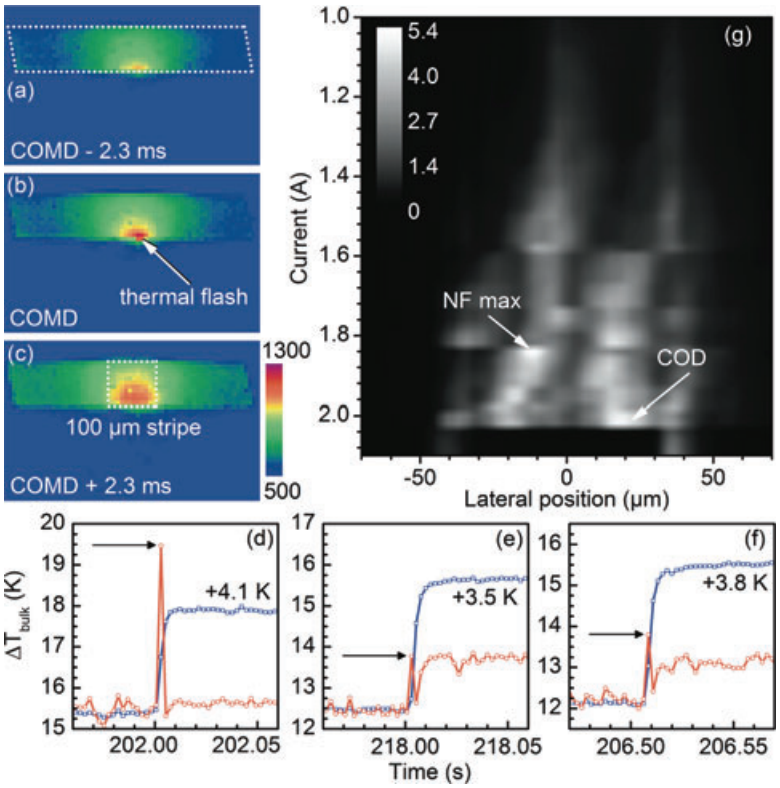

Figure 8 (online color at: www.lpr-journal.org) Data of red-emitting devices during cw operation according to Ziegler et al. [151]. Thermal images: (a) 2.3 ms (i. e., one camera frame) before COD (device shape is marked by dotted lines); (b) at COD, exhibiting a distinct thermal flash (marked by arrow); and (c) 2.3 ms after COD. (d-f) Temperature increases of three diode lasers showing the reproducibility of the observations. Notice (d) corresponds to the device from (a–c). Gray lines and symbols correspond to an average temperature of the 100-µm active stripe shown in (c); black lines and symbols correspond to the thermal flash in (b). (g) Nearfield versus current; arrows mark situations addressed in the text.

the lower and nominally doped regions adjacent to the QWs heat during device operation, which increases the rate of anion-vacancy defect formation. The associated formation of surface states has been identified to trigger the onset of COD. Thus, this approach provides a valuable contribution for the understanding of the first phase of COD.

COD in 650 nm emitting BA lasers with a stripe width of 100 µm has been investigated by Ziegler et al. [74, 151] in $L-I$-type experiments. Figures 8a–c show thermal images 2.3 ms before, directly at, and 2.3 ms after the onset of the thermal runaway. A pronounced 'thermal flash' shorter than 2.3 ms in duration is observed at the location where the thermal runaway ignites, followed by a jump of the temperature of the entire device. Nearfield data vs. current are shown in Fig. 8g. A two-lobe-nearfield, as typical for BA devices, is observed. With increasing current, the location of the power maximum jumps from one lobe to the other. The COD does not occur at the location with the highest absolute optical power (lateral position 12 µm, $P \sim 5.39$ a. u. at $I = 1.84$ A, $T_{\mathrm{bulk}} = 46.9$ °C), but at a 4 percent lower power with elevated bulk temperature in the other lobe (lateral position 24 µm, $P \sim 5.17$ a. u. at $I = 2.02$ A, $T_{\mathrm{bulk}} = 51.5$ °C); for details see also [30]. This confirms the concept that T_{crit} is fed by bulk and surface heating, the latter being proportional to P. Figures 8d–f show the overall reproducibility of the results including the presence of a 'thermal flash' between 2.0 and 2.2 A as obtained from 3 different devices of one batch. In general, a strict one-by-one correlation between thermal flashes and nearfield minima after COD (degradation signatures) was found. The identification of the thermal runaway processes by the observation of 'thermal flashes' paved the way for further use of thermography in COD analysis.

The results obtained by Jacob et al. [92] (Fig. 6) provide a substantial contribution in order to push the temporal resolution of the COD into the µs range. The visualization of the propagation of a 'defect front' and the observation of its deceleration towards zero confirms the picture of a third phase of COD as described in Sect. 1.1. Another topic of this work was the idea of COD fault protection. This has been accomplished by detecting voltage and current transients with µs-temporal resolution and temporarily removing electrical power from laser diodes according to the observation of pre-COD-signatures in voltage and current. This approach was claimed to increase the device lifetime by a factor of approximately two [92].

Further work aiming for COD prediction has been published by Maiorov et al. [72]. The authors use single µs-pulses and monitor emission power transients in and off center of the far field. A correlation between transient far-field broadening and P_{COD} has been discovered and used for non-destructive pre-testing of devices up to power levels as close as 90 percent of P_{COD}.

Ziegler et al. [87] reported single pulse COD tests. The motivation for using single pulses was to minimize the gradual aging that accompanies any type of device operation. For each single 2-µs-pulse the nearfield and a thermocamera image were monitored, both being temporally averaged across the pulse duration. Such data is shown in Fig. 9a,b and c,d for two individual devices. Thermal images taken during the first pulse and showing pronounced 'thermal flashes' (see Fig. 9a,c) are presented together with nearfields monitored in the first and second pulse (see Fig. 9b,d). Notice that there were no 'thermal flashes' during the second pulse (not shown). A clear correlation between 'thermal flashes'

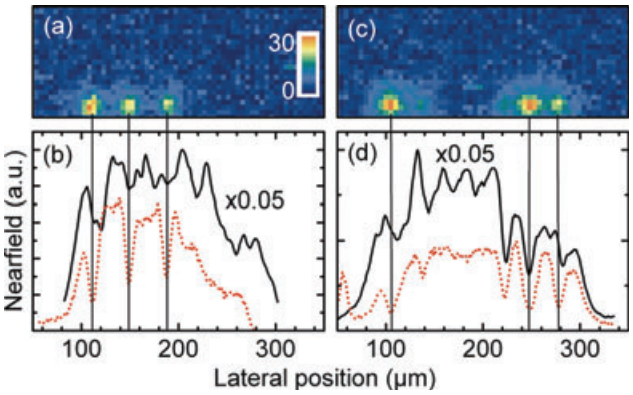

Figure 9 (online color at: www.lpr-journal.org) COD test carried out with two individual devices, where each has been subjected to two single rectangular current pulses of 35 A and 2 µs duration according to Ziegler et al. [87]. (a,c) represent the thermal images during the first pulse, while the ones taken during the second pulse are empty (and not shown here). (b,d) show the nearfields during first and second pulse as full and dotted lines, respectively.

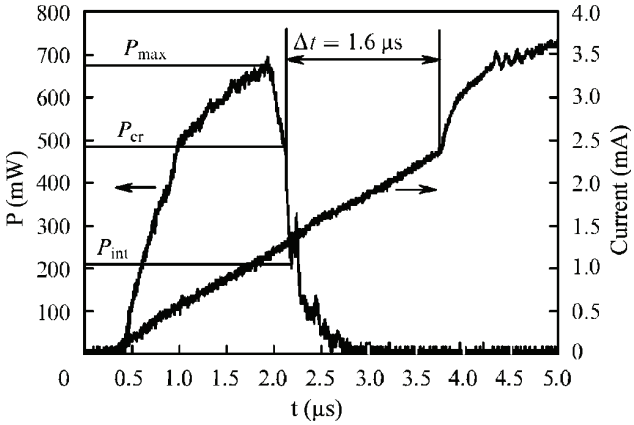

Figure 10 Time dependence of emission power (left ordinate) and pump current (right ordinate) in a single 6 µs saw-tooth pulse according to Miftakhutdinov et al. [49]. Emission power levels in different phases of the power transient are labeled.

and nearfield minima in the second pulse was found, while the correlation between 'thermal flashes' and nearfield minima in the first pulse was substantially poorer (vertical lines in Fig. 9). During the second pulse, the device is severely damaged already, in particular at the locations, where the thermal flashes have been observed during the first pulse. This results in the strong correlation between thermal flashes and nearfield minima. During the first pulse the situation is different: in the beginning, *high nearfield* intensities lead to strong local heating. As in the cw case discussed above, the thermal runaway ignites at the nearfield maxima. After this very short (compared to the 2 µs pulse length) process, the device is damaged at these particular locations. This structural damage leads to a locally *lowered nearfield* during the first pulse. The temporal averaging, however, is expected to merge both opposite effects, resulting in the weaker correlation for the first pulse. This fact clearly calls for experiments with increased temporal resolution.

Early pulsed COD measurements [7, 15, 26, 79, 80] provided valuable information about COD on the nanosecond timescale (Fig. 4b), even without temporally resolving any individual COD event. Achieving the latter goal requires single pulse COD measurements. Single-pulse experiments also minimize all gradual aging that accompanies device operation and potentially allow for distinguishing effects related to gradual aging and to COD. Both et al. [160] have analyzed the damage pattern after excitation with single nanosecond pulses of various energies, while Sim et al. [161] have employed single pulses to study the effect of electrostatic discharge on devices. They observed COD as one among other degradation modes caused by electrostatic discharge for forward bias of the device.

Miftakhutdinov et al. [49] have analyzed emission power transients of several batches of QW ridge-waveguide lasers during COD, which has been provoked by single saw-tooth pulses of 6 µs duration. Emission powers and currents were monitored during these pulses with a 2 ns temporal resolution. Figure 10 shows such data. After the emission power reaching its maximum, the authors observed a fast power decay within a *few tens of ns* followed by a decrease to the spontaneous emission level lasting *several hundred ns*. Within $\Delta t = 1.6$ µs, a jump in the pump current was observed that is interpreted as the irreversible creation of a shunting channel being likely related to the front facet damage. For different samples, Δt varied from almost zero up to the length of the current pulse. For some samples shunting channels did not appear. Diode lasers with an intermediate ZnSe layer in-between the as-cleaved facet and the coating forming the output mirror were found to have 1.5–2 times higher P_{COD}. This has been attributed to the additional heat-sinking effect of the ZnSe layer.

Elliott et al. [86] have performed a set of COD experiments by applying single rectangular current pulses. The changing light intensity during COD of the red-emitting QW based diode lasers was analyzed on a timescale of tens of nanoseconds. Using as-cleaved facets in the AlGaInP-system, which is notably susceptible to COD, the drop in light intensity and the area of damage to the facet were recorded as a function of current. In the current range up to 40 A, the total COD process up to the drop of light intensity to non-lasing levels took place on a timescale of hundreds of nanoseconds, approaching a limiting value of 200 ns. The measured area of facet damage showed a clear increase with current. Furthermore, the COD was accompanied by kinks in the operation current transients.

Ziegler et al. [152] have increased the temporal resolution of their experiment by replacing the CCD camera by a photodiode with a rise time of 1 ns. BA lasers emitting at 808 nm were analyzed. Figure 11 shows current and *spatially averaged* power transients (left panel) obtained in single-pulse-experiments while the right panel gives *temporally averaged* thermal images. The presence or absence of the thermal runaway is unambiguously detected by the thermocamera. Furthermore, this data demonstrates a t_{COD} value of a few tens of nanoseconds for sufficiently high operation currents. Such data are compiled in Fig. 12a. P_{COD}-values

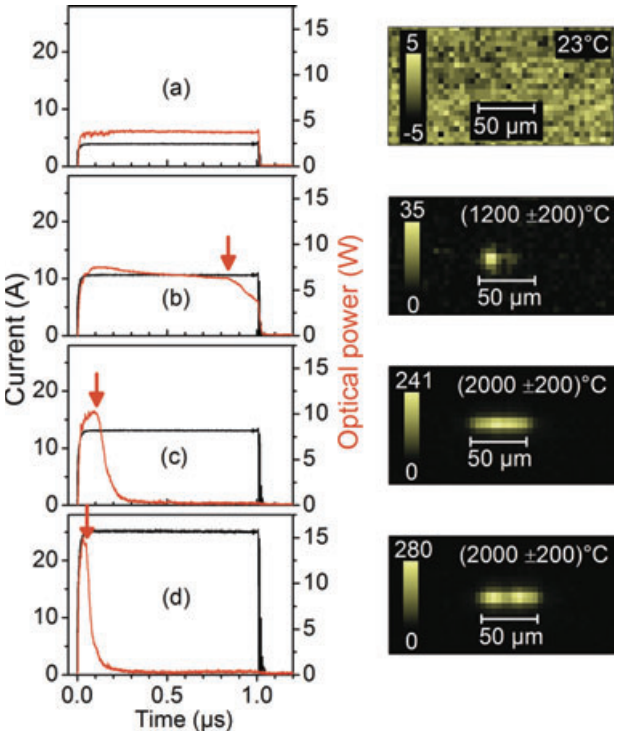

Figure 11 (online color at: www.lpr-journal.org) (a–d) Current and emission power transients from four individual devices according to Ziegler et al. [152]. Black lines (left ordinate) represent operation current transients, while red lines (right ordinate) indicate optical output power transients. The onset of the thermal runaway at t_{COD} is marked by arrows. The right panel shows the corresponding thermal images recorded during the entire current pulse. Estimated maximal temperatures of the thermal flashes are included. This estimation includes effects related to spatial and temporal averaging.

are plotted as full circles in case a thermal flash was observed. Open circles represent experiments where no COD and no thermal flash was detected. For this case, the ordinate gives the pulse length. Obviously, there is a borderline dividing the diagram (and hence the operation regimes) into two regions: one with and one without COD. The blurred region in-between is explained by the scattering of individual device properties within the sample set. The dashed line shows the 'square-root law' (cf. Figure 4b). Thus, compliance with the data obtained in pulsed operation (with multiple pulses) is demonstrated. Such a diagram defines regimes in which COD is avoided by the proper choice of operation parameters for a particular batch of devices. It is important to note that the t_{COD} scale is determined by the accumulation time of excess energy which is absorbed from the optical output and results eventually in a local melting of the device. This has been proven by making-up the energy balance within the tiny heated front facet volume (see Fig. 12c). The experimental value W_{exp} as derived from data sets such as given in Fig. 11 is compared with the energy required to reach T_m within this region. Linearity over two orders of magnitude is demonstrated.

Monitoring a COD diagram (see Fig. 12a) requires a homogeneous set of devices which eventually gets destroyed. Hempel et al. [24] have published an alternative approach based on a less complex step test with single, subsequently increasing current pulses. Before increasing the current by a further step, an additional test measurement with a regular operation current is made. This method was demonstrated with 975 nm emitting BA lasers. Figure 13 summarizes the results from 4 devices. Figure 13a shows the power evolution in test pulses and Fig. 13b quantifies the thermal flashes. There is a clear correlation between device degradation (power drop in the test pulse) and the first appearance of a 'thermal flash'. Most striking, however, is the finding of *multiple thermal flashes* giving direct evidence of the presence of multiple thermal runaway processes in subsequent pulses (cf. Sect. 2.2). Figure 13c shows even a lateral motion of the flash across about half of the emitter stripe width. For these devices the onset of the thermal runaway process is seen as thermal flash but not as distinct power drop, as observed for shorter wavelength devices [49, 86, 152] (see Figs. 10 and 11). The time constant of power loss for the 975 nm emitting devices was determined to 400–2000 ns, while Ziegler et al. [152] reported 30–400 ns for 808 nm emitting devices. This is in agreement with the empirically known higher robustness of longer wavelength devices against COD.

By using COD step tests, Hempel et al. [25] compared the COD behavior of devices with facets having different surface recombination velocities. For devices with the lowest surface recombination velocities, the asymmetry of the carrier profile (caused originally by the asymmetric coating) is enhanced and the bulk temperature close to the rear facet notably increases compared to the front section. This is caused by Auger recombination [106]. Although the thermal runaway remains the trigger of the COD, the Auger heating of the bulk close to the rear facet substantially contributes to the total rear facet temperature and thus promotes COD there. Thus, for high-quality devices, the rear facet may become the bottleneck for the overall performance and therefore requires additional attention.

The COD single-pulse step test bears the potential to become a standard COD test, because it reduces at the same time the expenses and effects related to thermal load and gradual aging.

5. Summary and Outlook

COD represents an important sudden degradation mechanism and major limit preventing diode lasers to reach ultrahigh emission powers. COD is controlled by thermal mechanisms extending over several orders of magnitude in time. This time flow can be separated into three phases (Fig. 14):

– In the 1st phase of COD the facet temperature is approaching a *critical temperature* T_{crit}. Depending on the surface status of the facet and on operation conditions this phase takes from years (higher and higher temperatures until T_{crit} is reached due to gradual material degradation under cw operation) down to a few tens of nanoseconds (temperature increase due to short high current pulse).

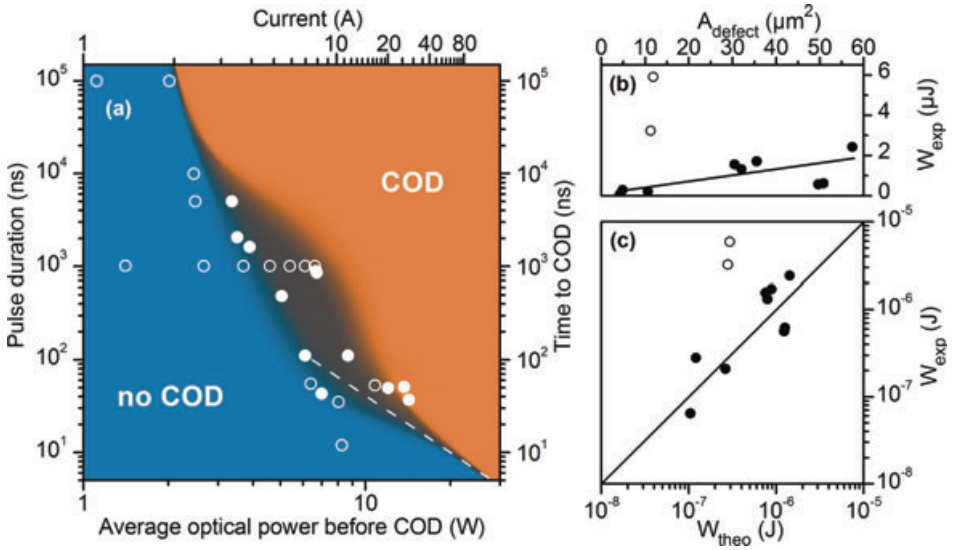

Figure 12 (online color at: www.lpr-journal.org) (a) Diagram showing the regions of COD (full circles) and no COD (open circles) occurrence for a batch of BA lasers (50 µm emitter stripe width) according to Ziegler et al. [152]. The presence of thermal runaway was concluded from analysis of thermal images such as displayed in Fig. 11 (right panel). The borderline (colored gray) is blurred because of the randomness in filamentation and scatter in properties of the involved devices. The dashed line indicates the 'square-root law'. (b) Absorbed output energy W_{exp} calculated from the experimental transients versus damaged area on the front facet (symbols). The solid line is to guide the eye. (c) Absorbed output energy W_{exp} as a function of the calculated thermal energy W_{theo} required for heating the damaged device volume to the melting point (symbols). Notice that open circles refer to tests with prologated pulses (5 and 100 µs), where heat removal during the pulse takes place.

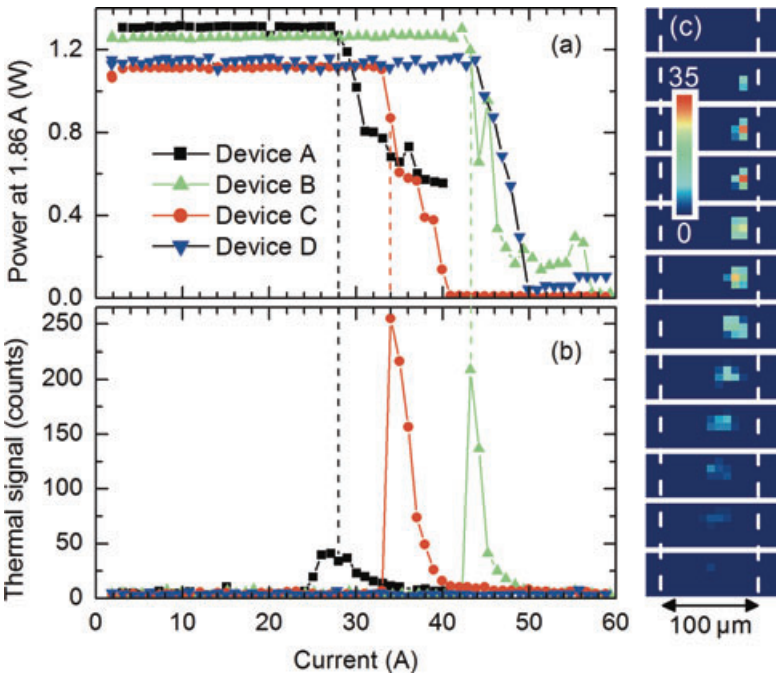

Figure 13 (online color at: www.lpr-journal.org) (a) Evolution of the optical output during a test current pulse of 1.86 A (as a measure of device degradation) for 4 devices after application of single current pulses with the amplitude given on the abscissa according to Hempel et al. [24]. (b) Intensity of the 'thermal flash' as recorded by the thermocamera. (c) Front facet thermal images taken from device A during subsequent pulses with amplitudes from 24 to 35 A (top to bottom). The emitter stripe width is indicated.

– The 2nd phase of COD involves the *thermal runaway*. Strongly localized melting takes place and the generated 'hot spot' spreads spatially. Model calculations predict rise times on the order of 1–10 ns. So far, this phase has never been experimentally resolved, but experimentally determined energy balances point to this timescale as well.

– The 3rd phase of COD begins when the thermal runaway stops because of a lack of energy. Further degradation, however, takes place, in particular if the operation current is not abruptly terminated. This represents the standard situation. This phase involves the creation of collateral damage such as dark bands that are not necessarily directly related to the primary damage event. The duration

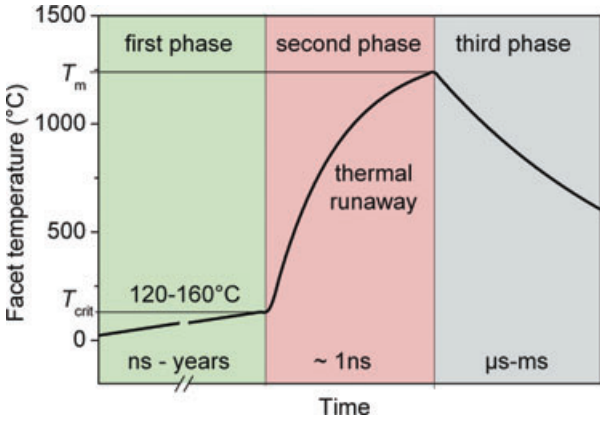

Figure 14 (online color at: www.lpr-journal.org) Schematic of the sequence of events during COD.

of this phase depends very much on operation conditions and might last up to minutes. Typical values are in the µs-ms range (if the operation current remains on). Further collateral damage can evolve even during days and weeks until the whole chip is damaged.

The particular feature of the thermal runaway mechanism is that a point-like microscopic source such as a single optical filament with a temperature in excess of T_{crit} is sufficient to make the entire macroscopic device collapsing. In BA laser diodes, such a filament will always be present at sufficient power levels.

For future work it will be important to temporally resolve COD further and to separate between the heat contributions involved into the process. Here, single pulse measurements on fresh diodes as well as on aged diodes are promising for the following reasons:

- The ratio between bulk and facet heating can be adjusted.
- Single-pulse operation helps for separating the role of the actual chip architecture from that of the thermal properties of the package.
- It allows for the intentional preparation of pre-stages and very early phases of the COD process. Devices intentionally degraded in such a way are interesting for further (destructive) analysis.
- COD can be analyzed even for diode lasers that fail under regular operation conditions by other mechanisms than COD.
- The single-pulse approach could help for establishing *standard COD-test procedures*. The dependence of COD on operation time (gradual degradation) can be studied.

Experimental challenges consist in the time resolved observation of the thermal runaway and the determination of the temporal temperature profile during the entire COD process. This involves also the temperature within the third phase.

Theory and modeling are required in order to explain the different COD kinetics observed for devices made of different material systems or operated under different conditions. Eventually, such work should lead to knowledge-based solutions that increase the optical strength of diode lasers against COD by design.

Acknowledgements. The authors would like to thank the following scientists for helpful discussions: Ute Zeimer, Bernd Sumpf, and Götz Erbert of the Ferdinand Braun Institute Berlin, Stella Elliott and Peter Smowton, of the University of Cardiff, Włodzimierz Nakwaski of the Technical University of Łódź, Martina Baeumler, of the Fraunhofer Institute for Applied Solid-State Physics Freiburg, Henning E. Larsen, Peter E. Andersen, and Paul M. Petersen of the Danish Technical University, Jose Manuel G. Tijero and Ignacio Esquivias of the Universidad Politecnica de Madrid, Michel Krakowski and Nicolas Michel of Alcatel-Thales III-V Lab Palaiseau, Julien Nagle of Thales Research and Technology Palaiseau, Peter Brick, Martin Reufer, Martin Müller, Harald König, and Uwe Strauss of Osram Opto Semiconductors Regensburg, and Marwan Bou Sanayeh of Notre Dame University Louaize, Lebanon. Funding by the European Commission within the project WWW.BRIGHTER.EU under Contract No. IST-2005-035266 is acknowledged.

Received: 20 September 2010, **Revised:** 19 January 2011, **Accepted:** 7 February 2011

Published online: 7 March 2011

Jens W. Tomm received Diploma and Ph. D. degree in Physics from Humboldt University Berlin, Germany. From 1993–1995 he was with Georgia Tech, Atlanta GA and 1999 with Riken, Sendai, Japan. In 1995, he became a member of the scientific staff of the newly founded Max Born Institute. There he runs the "Optoelectronic Device" group. His research interests include photonics, optoelectronics, and semiconductor physics.

Mathias Ziegler studied physics at Humboldt University in Berlin. At the Max Born Institute in Berlin he performed his doctoral work on optical and thermal properties of high-power laser diodes and did major contributions to establish thermography for testing semiconductor lasers. In 2009, he received a Ph. D. from the Humboldt University in Berlin. In 2010, he joined the BAM Federal Institute for Materials Research and Testing in Berlin, where his research is focused on the development of thermographic methods for non-destructive testing.

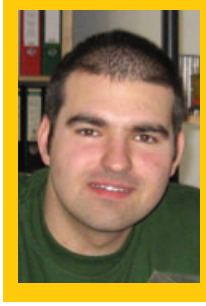

Martin Hempel studied physics at the Humboldt University in Berlin, finishing in 2009 with his diploma thesis about quantum cascade lasers. After that he joined the Max Born Institute in Berlin. There he is currently working on his Ph. D. focusing on optoelectronic devices and especially on the COD effect.

Thomas Elsaesser studied physics at the University of Heidelberg and the Technical University of Munich, Germany. He received a Dr. rer. nat. degree from the TU Munich in 1986. After working as a research associate at the TU Munich and spending a postdoc period at AT&T Bell Laboratories, Holmdel, USA, he finished his habilitation at the TU Munich in 1991. Since 1993, Dr. Elsaesser is a director of the Max Born Institute, holding a joint appointment with the Institute of Physics of Humboldt University, Berlin. He has contributed to a broad range of research in ultrafast science with processes in condensed matter representing the main area of his scientific work. Major topics are transient structures of as well as basic microscopic interactions and nonequilibrium dynamics in (bio)molecular systems and in solids, in particular semiconductors.

References

[1] A. Knigge, G. Erbert, J. Jonsson, W. Pittroff, R. Staske, B. Sumpf, M. Weyers, and G. Trankle, Electron. Lett. **41**, 250–251 (2005).
[2] H. X. Li, T. Towe, I. Chyr, D. Brown, T. Nguyen, F. Reinhardt, X. Jin, R. Srinivasan, M. Berube, T. Truchan, R. Bullock, and J. Harrison, IEEE Photon. Technol. Lett. **19**, 960–962 (2007).
[3] C. Harder, in: Optical Fiber Telecommunications V A Components and Subsystems, edited by I. P. Kaminov, T. Li, and A. E. Willner (Elsevier, Amsterdam, 2008), pp. 107–122.
[4] D. P. Cooper, C. H. Gooch, and R. J. Sherwell, IEEE J. Quantum Electron. **QE2**, 329–330 (1966).
[5] H. Kressel and H. Mierop, J. Appl. Phys. **38**, 5419–5421 (1967).
[6] C. H. Henry, P. M. Petroff, R. A. Logan, and F. R. Merritt, J. Appl. Phys. **50**, 3721–3732 (1979).
[7] P. G. Eliseev, J. Luminesc. **7**, 338–356 (1973).
[8] W. Nakwaski, J. Appl. Phys. **57**, 2424–2430 (1985).
[9] P. G. Eliseev, Prog. Quant. Electron. **20**, 1–82 (1996).
[10] W. R. Smith, J. Appl. Phys. **87**, 8276–8285 (2000).
[11] W. C. Tang, H. J. Rosen, P. Vettiger, and D. J. Webb, Appl. Phys. Lett. **58**, 557–559 (1991).
[12] G. Chen and C. L. Tien, J. Appl. Phys. **74**, 2167–2174 (1993).
[13] R. Schatz and C. G. Bethea, J. Appl. Phys. **76**, 2509–2521 (1994).
[14] T. Shibutani, M. Kume, K. Hamada, H. Shimizu, K. Itoh, G. Kano, and I. Teramoto, IEEE J. Quantum Electron. **23**, 760–764 (1987).
[15] T. Kamejima and H. Yonezu, Jpn. J. Appl. Phys. **19**, 425–429 (1980).
[16] M. Ziegler, V. Talalaev, J. W. Tomm, T. Elsaesser, P. Ressel, B. Sumpf, and G. Erbert, Appl. Phys. Lett. **92**, 203506 (2008).
[17] W. C. Tang, H. J. Rosen, P. Vettiger, and D. J. Webb, Appl. Phys. Lett. **59**, 1005–1007 (1991).
[18] J. S. Yoo, H. H. Lee, and P. Zory, IEEE J. Quantum Electron. **28**, 635–639 (1992).
[19] W. C. Tang, H. J. Rosen, P. Vettiger, and D. J. Webb, Appl. Phys. Lett. **60**, 1043–1045 (1992).
[20] F. A. Houle, D. L. Neiman, W. C. Tang, and H. J. Rosen, J. Appl. Phys. **72**, 3884–3896 (1992).
[21] A. Chavan, R. Radionova, G. W. Charache, R. J. Menna, H. Schluter, and J. L. Hostetler, IEEE J. Quantum Electron. **41**, 630–635 (2005).
[22] J. Hashimoto, I. Yoshida, M. Murata, and T. Katsuyama, IEEE J. Quantum Electron. **33**, 66–70 (1997).
[23] T. Fukushima, A. Furuya, Y. Kito, H. Sudo, M. Sugano, and T. Tanahashi, Electron. Commun. Jpn. 2, Electron. **78**, 11–19 (1995).
[24] M. Hempel, M. Ziegler, J. W. Tomm, T. Elsaesser, N. Michel, and M. Krakowski, Appl. Phys. Lett. **96**, 251105 (2010).
[25] M. Hempel, J. W. Tomm, M. Ziegler, T. Elsaesser, N. Michel, and M. Krakowski, Appl. Phys. Lett. **97**, 231101 (2010).
[26] J. S. Yoo, H. H. Lee, and P. S. Zory, IEEE Photon. Technol. Lett. **3**, 594–596 (1991).
[27] M. Fukuda, Reliability and Degradation of Semiconductor Lasers and LEDs, 1. ed. (Artech House Publishers, Norwood, 1991).
[28] P. W. Epperlein and O. J. F. Martin, Institute of Physics Conference Series **120**, 353–358 (1992).
[29] A. Moser and E. E. Latta, J. Appl. Phys. **71**, 4848–4853 (1992).
[30] J. W. Tomm, M. Ziegler, V. Talalaev, C. Matthiesen, T. Elsaesser, M. BouSanayeh, P. Brick, and M. Reufer, SPIE Proc. **7230**, 72300V-9 (2009).
[31] P. G. Eliseev, Reliability Problems of Semiconductor Lasers, Vol. 197 (Nova Science Publishers, Inc., Commack, New York, 1991).
[32] P. S. Cross, G. L. Harnagel, W. Streifer, D. R. Scifres, and D. F. Welch, Science **237**, 1305–1309 (1987).
[33] M. Sakamoto, D. F. Welch, J. G. Endriz, E. P. Zucker, and D. R. Scifres, Electron. Lett. **25**, 972–973 (1989).
[34] H. Brugger and P. W. Epperlein, Appl. Phys. Lett. **56**, 1049–1051 (1990).
[35] P. W. Epperlein, G. L. Bona, and P. Roentgen, Appl. Phys. Lett. **60**, 680–682 (1992).
[36] A. Oosenbrug and E. E. Latta, in: Proceedings of the LEOS '94 Lasers and Electro-Optics Society Annual Meeting, Vol. 2, Boston, MA 1994, pp. 37–38.
[37] A. Jakubowicz, Mater. Sci. Eng. B **44**, 359–363 (1997).
[38] A. Moser, E. E. Latta, and D. J. Webb, Appl. Phys. Lett. **55**, 1152–1154 (1989).
[39] P. W. Epperlein and G. L. Bona, Appl. Phys. Lett. **62**, 3074–3076 (1993).
[40] P. W. Epperlein, P. Buchmann, and A. Jakubowicz, Appl. Phys. Lett. **62**, 455–457 (1993).
[41] G. Beister, J. Maege, D. Gutsche, G. Erbert, J. Sebastian, K. Vogel, M. Weyers, J. Wurfl, and O. P. Daga, Appl. Phys. Lett. **68**, 2467–2468 (1996).
[42] P. Ressel, G. Erbert, U. Zeimer, K. Hausler, G. Beister, B. Sumpf, A. Klehr, and G. Trankle, IEEE Photon. Technol. Lett. **17**, 962–964 (2005).
[43] L. W. Tu, E. F. Schubert, M. Hong, and G. J. Zydzik, J. Appl. Phys. **80**, 6448–6451 (1996).
[44] H. Ichikawa, C. Fukuda, K. Hamada, and T. Nakabayashi, Jpn. J. Appl. Phys. **47**, 7890–7895 (2008).
[45] H. Horie, H. Ohta, and T. Fujimori, IEEE J. Sel. Top. Quantum Electron. **5**, 832–838 (1999).

[46] R. W. Lambert, T. Ayling, A. F. Hendry, J. M. Carson, D. A. Barrow, S. McHendry, C. J. Scott, A. McKee, and W. Meredith, J. Lightwave Technol. **24**, 956–961 (2006).
[47] S. Kamiyama, Y. Mori, Y. Takahashi, and K. Ohnaka, Appl. Phys. Lett. **58**, 2595–2597 (1991).
[48] G. Beister, J. Maege, J. Sebastian, G. Erbert, L. Weixelbaum, M. Weyers, J. Wurfl, and O. P. Daga, IEEE Photon. Technol. Lett. **8**, 1124–1126 (1996).
[49] D. R. Miftakhutdinov, I. V. Akimova, A. P. Bogatov, T. I. Gushchik, A. E. Drakin, N. V. D'Yachkov, V. V. Popovichev, and A. P. Nekrasov, Quantum Electron. **38**, 993–1000 (2008).
[50] F. U. Herrmann, S. Beeck, G. Abstreiter, C. Hanke, C. Hoyler, and L. Korte, Appl. Phys. Lett. **58**, 1007–1009 (1991).
[51] H. Horie, Y. Yamamoto, N. Arai, and H. Ohta, IEEE Photon. Technol. Lett. **12**, 13–15 (2000).
[52] F. Rinner, J. Rogg, M. T. Kelemen, M. Mikulla, G. Weimann, J. W. Tomm, E. Thamm, and R. Poprawe, J. Appl. Phys. **93**, 1848–1850 (2003).
[53] J. Hashimoto, T. Katsuyama, I. Yoshida, M. Murata, and H. Hayashi, Electronics Letters **30**, 1146–1147 (1994).
[54] H. O. Yonezu, M. Ueno, T. Kamejima, and I. Hayashi, IEEE J. Quantum Electron. **15**, 775–781 (1979).
[55] C. L. Walker, A. C. Bryce, and J. H. Marsh, IEEE Photon. Technol. Lett. **14**, 1394–1396 (2002).
[56] H. Taniguchi, H. Ishii, R. Minato, Y. Ohki, T. Namegaya, and A. Kasukawa, IEEE J. Sel. Top. Quantum Electron. **13**, 1176–1179 (2007).
[57] P. G. Piva, S. Fafard, M. Dion, M. Buchanan, S. Charbonneau, R. D. Goldberg, and I. V. Mitchell, Appl. Phys. Lett. **70**, 1662–1664 (1997).
[58] P. G. Piva, R. D. Goldberg, I. V. Mitchell, S. Fafard, M. Dion, M. Buchanan, S. Charbonneau, G. Hillier, and C. Miner, J. Vac. Sci. Technol. B **16**, 1790–1793 (1998).
[59] H. C. Ko, M. W. Cho, J. H. Chang, and M. Yang, Appl. Phys. A Mater. Sci. Proc. **68**, 467–470 (1999).
[60] F. R. Gfeller, P. Buchmann, P. W. Epperlein, H. P. Meier, and J. P. Reithmaier, J. Appl. Phys. **72**, 2131–2135 (1992).
[61] J. Ungar, N. Barchaim, and I. Ury, Electron. Lett. **22**, 279–280 (1986).
[62] R. L. Thornton, D. F. Welch, R. D. Burnham, T. L. Paoli, and P. S. Cross, Appl. Phys. Lett. **49**, 1572–1574 (1986).
[63] http://www.intenseco.com/technology/.
[64] D. Botez, Appl. Phys. Lett. **74**, 3102–3104 (1999).
[65] I. B. Petrescu-Prahova, P. Modak, E. Goutain, D. Silan, D. Bambrick, J. Riordan, T. Moritz, S. D. McDougall, B. Qiu, and J. H. Marsh, SPIE Proc. **7198**, 71981I (2009).
[66] J. Pomplun, S. Burger, F. Schmidt, A. Schliwa, D. Bimberg, A. Pietrzak, H. Wenzel, and G. Erbert, Phys. Stat. Sol. B **247**, 846–853 (2010).
[67] M. V. Maximov, Y. M. Shernyakov, I. I. Novikov, L. Y. Karachinsky, N. Y. Gordeev, U. Ben-Ami, D. Bortman-Arbiv, A. Sharon, V. A. Shchukin, N. N. Ledentsov, T. Kettler, K. Posilovic, and D. Bimberg, IEEE J. Sel. Top. Quantum Electron. **14**, 1113–1122 (2008).
[68] B. Corbett, P. Lambkin, J. O'Callaghan, S. Deubert, W. Kaiser, J. P. Reithmaier, and A. Forchel, IEEE Photon. Technol. Lett. **19**, 916–918 (2007).
[69] J. N. Walpole, J. P. Donnelly, P. J. Taylor, L. J. Missaggia, C. T. Harris, R. J. Bailey, A. Napoleone, S. H. Groves, S. R. Chinn, R. Huang, and J. Plant, IEEE Photon. Technol. Lett. **14**, 756–758 (2002).
[70] J. P. Donnelly, R. K. Huang, J. N. Walpole, L. J. Missaggia, C. T. Harris, J. J. Plant, R. J. Bailey, D. E. Mull, W. D. Goodhue, and G. W. Turner, IEEE J. Quantum Electron. **39**, 289–298 (2003).
[71] P. K. L. Chan, K. P. Pipe, J. J. Plant, R. B. Swint, and P. W. Juodawlkis, Appl. Phys. Lett. **89** (2006).
[72] M. Maiorov, D. Damm, I. Trofimov, V. Zeidel, and R. Sellers, SPIE Proc. **7434**, 743404 (2009).
[73] M. BouSanayeh, P. Brick, W. Schmid, B. Mayer, M. Muller, M. Reufer, K. Streubel, J. W. Tomm, and G. Bacher, Appl. Phys. Lett. **91**, 041115 (2007).
[74] M. Ziegler, J. W. Tomm, T. Elsaesser, C. Matthiesen, M. BouSanayeh, and P. Brick, Appl. Phys. Lett. **92**, 103514 (2008).
[75] S. J. Sweeney, L. J. Lyons, A. R. Adams, and D. A. Lock, IEEE J. Sel. Top. Quantum Electron. **9**, 1325–1332 (2003).
[76] A. Moser, A. Oosenbrug, E. E. Latta, T. Forster, and M. Gasser, Appl. Phys. Lett. **59**, 2642–2644 (1991).
[77] T. Q. Tien, F. Weik, J. W. Tomm, B. Sumpf, M. Zorn, U. Zeimer, and G. Erbert, Appl. Phys. Lett. **89**, 181112 (2006).
[78] A. Moser, Appl. Phys. Lett. **59**, 522–524 (1991).
[79] H. Fujii, Y. Ueno, and K. Endo, Appl. Phys. Lett. **62**, 2114–2115 (1993).
[80] F. Kappeler, K. Mettler, and K. H. Zschauer, IEE Proc. I, Commun. Speech Vis. **129**, 256–261 (1982).
[81] D. Lock, S. J. Sweeney, and A. R. Adams, Phys. Stat. Sol. B **241**, 3416–3419 (2004).
[82] S. Mahajan, H. Temkin, and R. A. Logan, Appl. Phys. Lett. **44**, 119–121 (1984).
[83] S. N. G. Chu, S. Nakahara, M. E. Twigg, L. A. Koszi, E. J. Flynn, A. K. Chin, B. P. Segner, and W. D. Johnston, J. Appl. Phys. **63**, 611–623 (1988).
[84] O. Ueda, K. Wakao, S. Komiya, A. Yamaguchi, S. Isozumi, and I. Umebu, J. Appl. Phys. **58**, 3996–4002 (1985).
[85] C. W. Snyder, J. W. Lee, R. Hull, and R. A. Logan, Appl. Phys. Lett. **67**, 488–490 (1995).
[86] S. N. Elliott, P. M. Smowton, M. Ziegler, J. W. Tomm, and U. Zeimer, J. Appl. Phys. **107**, 123116 (2010).
[87] M. Ziegler, J. W. Tomm, D. Reeber, T. Elsaesser, U. Zeimer, H. E. Larsen, P. M. Petersen, and P. E. Andersen, Appl. Phys. Lett. **94**, 191101 (2009).
[88] I. Rechenberg, A. Hopner, J. Maege, A. Klein, G. Beister, and M. Weyers, Inst. Phys. Conf. Ser. Microsc. Semicond. Mater. **146**, 587–590 (1995).
[89] R. E. Mallard and R. Clayton, SPIE Proc. **3004**, 145–150 (1997).
[90] M. BouSanayeh, A. Jaeger, W. Schmid, S. Tautz, P. Brick, K. Streubel, and G. Bacher, Appl. Phys. Lett. **89** (2006).
[91] T. S. Yeoh, J. A. Chaney, M. S. Leung, N. A. Ives, Z. D. Feinberg, J. G. Ho, and J. U. Wen, J. Appl. Phys. **102** (2007).
[92] J. H. Jacob, R. Petr, M. A. Jaspan, S. D. Swartz, M. T. Knapczyk, and A. M. Flusberg, SPIE Proc. **7198**, 719815 (2009).
[93] A. K. Chin, R. K. Bertaska, M. A. Jaspan, A. M. Flusberg, S. D. Swartz, M. T. Knapczyk, R. Petr, I. Smilanski, and J. H. Jacob, SPIE Proc. **7198**, 71981A (2009).
[94] M. Baeumler, J. L. Weyher, S. Muller, W. Jantz, R. Stibal, G. Herrmann, J. Luft, K. Sporrer, and W. Spath, in: Defect Recognition and Image Processing in Semiconductors 1997, Vol. 160, edited by J. Donnecker and I. Rechenberg (Institute of Physics (IOP), Templin, Germany, 1998), pp. 467–470.

[95] C. Frigeri, M. Baeumler, A. Migliori, S. Muller, J. L. Weyher, and W. Jantz, Mater. Sci. Eng. B, Solid State Mater. Adv. Technol. **66**, 209–214 (1999).
[96] D. R. Pendse, in: Proceedings of the LEOS' 96 Lasers and Electro-Optics Society Annual Meeting, Vol. 1 (IEEE, Boston MA, 1996), pp. 354–355.
[97] T. Q. Tien, A. Gerhardt, S. Schwirzke-Schaaf, J. W. Tomm, M. Pommies, M. Avella, J. Jimenez, M. Oudart, and J. Nagle, Appl. Phys. Lett. **87**, 211110 (2005).
[98] M. B. Sanayeh, Thesis, Universität Duisburg-Essen, 2008.
[99] V. M. Glazov, S. N. Chizhevskaya, and N. y. N. Glagoleva, Liq. Semiconduct. (Plenum Press, New York, 1969).
[100] K. H. Park, J. K. Lee, D. H. Jang, H. S. Cho, C. S. Park, K. E. Pyun, J. Y. Jeong, S. Nahm, and J. Jeong, Appl. Phys. Lett. **73**, 2567–2569 (1998).
[101] D. H. Jang, J. K. Lee, K. H. Park, H. S. Cho, E. S. Nam, C. S. Park, J. I. Shim, J. C. Jeong, K. T. Jeong, and S. J. Park, Jpn. J. Appl. Phys. 1 **38**, 4756–4763 (1999).
[102] M. Ziegler, R. Pomraenke, M. Felger, J. W. Tomm, P. Vasa, C. Lienau, M. BouSanayeh, A. Gomez-Iglesias, M. Reufer, F. Bugge, and G. Erbert, Appl. Phys. Lett. **93**, 041101 (2008).
[103] B. W. Hakki and F. R. Nash, J. Appl. Phys. **45**, 3907–3912 (1974).
[104] R. E. Mallard, R. Clayton, D. Mayer, and L. Hobbs, J. Vac. Sci. Technol. A **16**, 825–829 (1998).
[105] E. C. Madhavamenon, P. M. Petroff, and R. G. Waters, Appl. Phys. Lett. **54**, 2683–2685 (1989).
[106] U. Menzel, Semiconduct. Sci. Technol. **13**, 265–276 (1998).
[107] R. Puchert, J. W. Tomm, A. Jaeger, A. Bärwolff, J. Luft, and T. W. Späth, Appl. Phys. A, Mater. Sci. Process. **66**, 483–486 (1998).
[108] S. Todoroki, M. Sawai, and K. Aiki, J. Appl. Phys. **58**, 1124–1128 (1985).
[109] R. Loudon, Adv. Phys. **13**, 423–482 (1964).
[110] J. W. Tomm, E. Thamm, A. Bärwolff, T. Elsaesser, J. Luft, M. Baeumler, S. Mueller, W. Jantz, I. Rechenberg, and G. Erbert, Appl. Phys. A, Mater. Sci. Process. **70**, 377–381 (2000).
[111] M. Kreissl, T. Q. Tien, J. W. Tomm, D. Lorenzen, A. Kozlowska, M. Latoszek, M. Oudart, and J. Nagle, Appl. Phys. Lett. **88**, 133510 (2006).
[112] W. C. Tang, H. J. Rosen, P. Buchmann, P. Vettiger, and D. Webb, J. Appl. Phys. **68**, 5930–5932 (1990).
[113] J. W. Tomm, F. Rinner, J. Rogg, E. Thamm, C. Ribbat, R. Sellin, and D. Bimberg, SPIE Proc. **4993**, 91–98 (2003).
[114] J. W. Tomm, A. Baerwolff, R. Puchert, A. Jaeger, and T. Elsaesser, in: Proc. SPIE **3244**, 576–586 (1998).
[115] S. Beeck, F. U. Herrmann, G. Abstreiter, C. Hanke, and L. Korte, Inst. Phys. Conf. Ser. **112**, 561–566 (1990).
[116] G. Abstreiter, Appl. Surface Sci. **50**, 73–78 (1991).
[117] P. W. Epperlein, Inst. Phys. Conf. Ser. **112**, 633–638 (1990).
[118] P. W. Epperlein, Jpn. J. Appl. Phys. 1 **32**, 5514–5522 (1993).
[119] T. J. Ochalski, D. Pierścińska, K. Pierściński, M. Bugajski, J. W. Tomm, T. Grunske, and A. Kozlowska, Appl. Phys. Lett. **89**, 071104 (2006).
[120] T. Hayakawa, Appl. Phys. Lett. **75**, 1467–1469 (1999).
[121] T. Hayakawa, M. Wada, F. Yamanaka, H. Asano, T. Kuniyasu, T. Ohgoh, and T. Fukunaga, Appl. Phys. Lett. **75**, 1839–1841 (1999).
[122] T. Ohgoh, T. Fukunaga, and T. Hayakawa, Electr. Eng. Jpn. **158**, 53–59 (2007).
[123] D. Wawer, T. J. Ochalski, T. Piwonski, A. Wojcik-Jedlinska, M. Bugajski, and H. Page, Phys. Stat. Sol. A, Appl. Mater. Sci. **202**, 1227–1232 (2005).
[124] P. K. L. Chan, K. P. Pipe, Z. Mi, J. Yang, P. Bhattacharya, and D. Luerssen, Appl. Phys. Lett. **89** (2006).
[125] M. Bugajski, T. Piwonski, D. Wawer, T. Ochalski, E. Deichsel, P. Unger, and B. Corbett, Mater. Sci. Semicond. Proc. **9**, 188–197 (2006).
[126] D. Pierścińska, K. Pierściński, M. Bugajski, and J. W. Tomm, Phys. Stat. Sol. A **204**, 422–429 (2007).
[127] D. Pierścińska, A. Kozlowska, K. Pierściński, M. Bugajski, J. W. Tomm, M. Ziegler, and F. Weik, J. Mater. Sci. Mater. Electron. **19**, S150-S154 (2008).
[128] K. Pierściński, D. Pierścińska, and M. Bugajski, Microelectronics J. **40**, 1373–1378 (2009).
[129] K. Pierściński, D. Pierścińska, K. Kosiel, A. Szerling, and M. Bugajski, J. Electron. Mater. **39**, 630–634 (2010).
[130] S. Dilhaire, S. Grauby, S. Jorez, L. D. P. Lopez, E. Schaub, and W. Claeys, Microelectronics Reliability **41**, 1597–1601 (2001).
[131] S. Dilhaire, S. Jorez, L. D. Patino-Lopez, W. Claeys, and E. Schaub, Microelectronics J. **32**, 899–901 (2001).
[132] E. Schaub, Jpn. J. Appl. Phys. 1 **40**, 2752–2756 (2001).
[133] D. Z. Garbuzov, N. Y. Antonishkis, A. D. Bondarev, A. B. Gulakov, S. N. Zhigulin, N. I. Katsavets, A. V. Kochergin, and E. V. Rafailov, IEEE J. Quantum Electron. **27**, 1531–1536 (1991).
[134] D. Z. Garbuzov, N. I. Katsavets, A. V. Kochergin, and V. B. Khalfin, in: AIP Conf. Proc. **240**, 6–13 (1991).
[135] N. I. Katsavets, D. Z. Garbuzov, T. A. Grishina, I. E. Kudrik, and P. V. Pitkianen, SPIE Proc. **2148**, 152–156 (1994).
[136] J. S. Yoo, M. S. Oh, H. S. Park, S. T. Jung, G. T. Park, and K. Y. Park, Jpn. J. Appl. Phys. 2 **31**, L1686–L1688 (1992).
[137] J. M. Rommel, P. Gavrilovic, and F. P. Dabkowski, J. Appl. Phys. **80**, 6547–6549 (1996).
[138] D. C. Hall, L. Goldberg, and D. Mehuys, Appl. Phys. Lett. **61**, 384–386 (1992).
[139] F. P. Dabkowski, A. K. Chin, P. Gavrilovic, S. Alie, and D. M. Beyea, Appl. Phys. Lett. **64**, 13–15 (1994).
[140] M. Bertolotti, G. Liakhou, R. Livoti, R. P. Wang, C. Sibilia, and V. P. Yakovlev, J. Appl. Phys. **74**, 7054–7060 (1993).
[141] M. Bertolotti, G. L. Liakhou, R. L. Voti, C. Sibilia, A. Syrbu, and R. P. Wang, Appl. Phys. Lett. **65**, 2266–2268 (1994).
[142] M. Ziegler, J. W. Tomm, T. Elsaesser, C. Monte, J. Hollandt, H. Kissel, and J. Biesenbach, J. Appl. Phys. **103**, 104508 (2008).
[143] J. LeClech, M. Ziegler, J. Mukherjee, J. W. Tomm, T. Elsaesser, J.-P. Landesman, B. Corbett, J. G. Mclnerney, J. P. Reithmaier, S. Deubert, A. Forchel, W. Nakwaski, and R. P. Sarzala, J. Appl. Phys. **105**, 014502 (2009).
[144] M. Passlack, C. G. Bethea, W. S. Hobson, J. Lopata, E. F. Schubert, G. J. Zydzik, D. T. Nichols, J. F. Dejong, U. K. Chakrabarti, and N. K. Dutta, IEEE J. Sel. Top. Quantum Electron. **1**, 110–116 (1995).
[145] J. Troger, M. Schwarz, and A. Jakubowicz, J. Lightwave Technol. **23**, 3889–3892 (2005).
[146] B. L. Meadows, F. Amzajerdian, N. R. Baker, V. Sudesh, U. N. Singh, and M. J. Kavaya, SPIE Proc. **5336**, 203–211 (2004).
[147] A. Kozlowska, M. Latoszek, J. W. Tomm, F. Weik, T. Elsaesser, M. Zbroszczyk, M. Bugajski, B. Spellenberg, and M. Bassler, Appl. Phys. Lett. **86**, 203503 (2005).

[148] A. Kozlowska, P. Wawrzyniak, J. W. Tomm, F. Weik, and T. Elsaesser, Appl. Phys. Lett. **87**, 153503 (2005).
[149] M. Ziegler, F. Weik, J. W. Tomm, T. Elsaesser, W. Nakwaski, R. P. Sarzala, D. Lorenzen, J. Meusel, and A. Kozlowska, Appl. Phys. Lett. **89**, 263506 (2006).
[150] M. Ziegler, J. W. Tomm, T. Elsaesser, G. Erbert, F. Bugge, W. Nakwaski, and R. P. Sarzala, Appl. Phys. Lett. **92**, 103513 (2008).
[151] M. Ziegler, J. W. Tomm, U. Zeimer, and T. Elsaesser, J. Electronic, Mater. **39**, 709–714 (2010).
[152] M. Ziegler, M. Hempel, H. E. Larsen, J. W. Tomm, P. E. Andersen, S. Clausen, S. N. Elliott, and T. Elsaesser, Appl. Phys. Lett. **97**, 021110 (2010).
[153] C. A. Hoffman, K. Jarasiunas, H. J. Gerritsen, and A. V. Nurmikko, Appl. Phys. Lett. **33**, 536–539 (1978).
[154] J. W. Tomm, A. Bärwolff, U. Menzel, M. Voss, R. Puchert, T. Elsaesser, F. X. Daiminger, S. Heinemann, and J. Luft, J. Appl. Phys. **81**, 2059–2063 (1997).
[155] W. Nakwaski, Opt. Quantum Electron. **21**, 331–334 (1989).
[156] W. Nakwaski, J. Appl. Phys. **67**, 1659–1668 (1990).
[157] D. R. Miftakhutdinov, A. P. Bogatov, and A. E. Drakin, Quantum Electron. **40**, 583–588 (2010).
[158] D. R. Miftakhutdinov, A. P. Bogatov, and A. E. Drakin, Quantum Electron. **40**, 589–595 (2010).
[159] R. J. Cobley, K. S. Teng, M. R. Brown, S. P. Wilks, and P. Rees, Appl. Phys. Lett. **91**, 081119 (2007).
[160] W. Both, G. Erbert, A. Klehr, R. Rimpler, G. Stadermann, and U. Zeimer, IEE Proc. J, Optoelectron. **134**, 95–103 (1987).
[161] S. P. Sim, M. J. Robertson, and R. G. Plumb, J. Appl. Phys. **55**, 3950–3955 (1984).